FRERES MENTOURI UNIVERSITY
CONSTANTINE 1 -ALGERIA

# Journal of Sciences & Technology

Semestrial Journal of Freres Mentouri University, Constantine, Algeria

VOLUME 04 - ISSUE 01— JUNE 2019

EISSN: ….-….

Freres Mentouri
University Constantine

Ain El-Bey Road
Constantine 25000
Algeria

Phone.Fax: 213 (0) 31. 81. 12.78
Email: revues@umc.edu.dz
Website :http://revue.umc.edu.dz

# Journal of Sciences & Technology

**Volume 4 N° 1 - June 2019**

**Semestrial Journal of Freres Mentouri Constantine 1 University, Algeria**





An article proposed for publication should not be submitted at the same time to another journal.

Manuscripts (original and two copies) should be sent to the following address:


Vice-Rectorate in charge of Post-Graduation and Scientific Research

Direction of Publications and Scientific Animation (15th floor)

Constantine 1 University , Aïn-El-Bey Road, 25000 Constantine, ALGERIA.

Tél./Fax: 213 (0) 31.81.12.78

**e-mail: revues@umc.edu.dz**

Constantine1 University

**Journal of Sciences & Technology**

Volume 4 N° 1 – June 2019

# SCIENTIFIC COMMITTEE

# INSTRUCTIONS TO AUTHORS

## I- Overview

The journal Human Sciences publishes in three languages: Arabic, French and English. Two abstracts must be provided, one in the language of the article, the other in Arabic if the article is written in another language, or in French (or English) if the article is written in Arabic. Abstracts must not exceed 150 words. Unpublished articles are not returned to their authors.

## II- Manuscrips

The articles submitted for publication (three copies) must not exceed 20 typewritten pages (tables, figures, graphs, bibliography, ... included) with a large margin to the left (3 cm), printed on 21 x 29 paper , 7 cm (A4) with interligne of good readability. Some flexibility is allowed to authors, but they should organize the text clearly in sections such as: Introduction, Experimental Details, Results, Discussion and Conclusion. The longer articles will be published by part in successive issues, each part being determined by the authors. Authors are kindly requested to accompany the summary of their articles with the most complete possible keywords.

In order to save time and respect deadlines for publication, it is recommended that authors take care of the complete capture of their article on a computer, and send it to the journal, after they have been informed. acceptance for publication, in the form of files on CD.ROM, which will be copied by the service.

However, since the final formatting of the article is done by P.A.O. (Computer Aided Publication), the authors are asked to avoid any formatting of their text. It will be necessary to avoid stylizing it.

## III- Bibliography

The bibliographic references quoted in the text must include only the reference number in square brackets (ex .: [5]). If the name of the author appears in the text, it must be followed by the reference number. When the reference contains more than two authors, only the first is cited, followed by "and al".

For articles, the complete reference includes the names of the authors followed by the initials of their first names, the title of the article, the title of the periodical (in conformity with the abbreviations allowed), the volume, the number of the periodical, the year of publication and the relevant pages.

For the works, the reference must include the names of the authors followed by the initials of their first names, the complete title of the work, the volume, the volume, the first and the last page relating to the results discussed, the number of the edition if there are several, the name of the publisher, the place and the year of edition.

For scientific meetings (congresses, proceedings, ...), the reference includes the names of the authors followed by the initials of their first names, the title of the communication, the identification of the meeting, the place, the period and the pages concerned.

## IV- Iconography

Tables, boards, charts, maps, photographs, etc. must be provided separately, inset. They must be presented on white sheets of A4 format, individually or in groups, and have underneath the words "table" or "figure" assigned a number.

The illustrations and figures must be clear, professionally made and adequate for reproduction: a 50% reduction, if any, must lead to a suitable size and thickness of characters for good readability. Moreover, for computer-generated figures, in order to maximize contrast, the use of a laser or inkjet printer is essential.

Legends assigned their numbers must be grouped in a separate page.

The final presentation of the article will be left to the discretion of the Editorial Board.

Journal of Sciences & Technology
Volume 4 N° 1– June 2019

# SUMMARY

SUMMARY



Journal of Sciences & Technology
Volume 4 N° 1– June 2019

# OXFORD NANOTECHNOLOGIE: A NEW ERA FOR GENOME SEQUENCING AND PRECISION DIAGNOCTICS

*Submited on 21/02/2019 – Accepted on 03/06/2019*

**Abstract**

The advancement made on sequencing technology over the last years has been impressive. However, a number of new instruments were commercialized, the most attractive and promising one was the MinIon from Oxford Nanopore technology, UK. It is a small USB device using the nanopore technology to sequence more than 100kbp of DNA single stranded in a short time without pre-amplification or optical steps. This review focusses on the use of the new sequencing technology to improve the molecular and the precision diagnostic. Herein, we expose the employment of MinIon device for characterization, monitoring and detection of mutations in infectious agents but also its application in precision diagnosis and mutation analysis in clinical oncology and immunologic research.

***Keywords :*** oxford, nanotechnologie, genome sequencing, precision diagnoctics.

**I. ELOUAR**

**A. DJEKOUN**

Frères Mentouri University
Constantine, Algeria.

## INTRODUCTION

For a long time medicine prescribes the same drugs to treat all patients that have the same disease. These drugs have shown efficacy in some patient but they have different side effect in other. Recently, research has shown that the efficacy and the metabolism of drugs differ from an individual to another depending on its genetic composition and environmental factors (Nebert et Zhang, 2019). Hence, nowadays the improvement of molecular diagnostics in routine clinical care is needful.

Gene sequencing has played an integral role in the advancement and understanding of disease pathology and treatment. A decade ago, a sequencing revolution was born with the advent of second-next generation sequencing (NGS). The most sold instruments are Illumina and Ion Torrent. The NGS technology works by detecting the incorporation of the labelled nucleotides directly without separation of DNA in a gel (Steinbock and Radenovic, 2015). Therefore, these technologies rely on multiple manipulation steps to covert native DNA in a form that can be detected using electrical or chemical signals by various sensing mechanisms. It is now clear that DNA manipulation can cause artifacts and inaccuracies in DNA measurements (Ozsolak,2012). In addition, each step limits them to short 100–400 bp read lengths due to inevitable phasing issues (when templates in a polymerase colony lose synchronicity). These shorter reads make genome, transcriptome, and metagenome assembly more challenging and leaves some areas of the human genome unresolvable (Leggett and Clark, 2017).

On the other hand, the established of these platforms are very expensive, immobile, and require regular maintenance, making them a costly inclusion on a research proposal or programmatic intervention grant in the developing countries.

The increasing demand for faster and cheaper genome sequencing results in the development of advanced sequencing technologies (Chaisson et al, 2015). Nanopore sequencing is belived to be one of the most promising sequencing technologies to reach foor gold standards set for the "$1000 Genome" project; targeted prevention, effective therapy, better vaccines, lower costs (wang et al, 2015). Effectively, nanopore sequencing has changed the NGS landscape with cheap portable sequencers, rapid simple library preparation (15 min), and automated real-time analysis. Those methods are valuable tools for clinical testing and could possibly enable small/mid-scale research centres and hospitals to conduct research studies by genotypic driver genes and selecting suitable therapeutic approaches (Norris, 2016).

This review is an overview of the new genomic sequencing instrument "oxford nanopore technology" and its clinical employment for microbiology and precision diagnostic in cancer and immunology research.

## 2- NANOPORE SEQUENCING

In 2003, the first complete inventory was taken of the building blocks of the human genome. Since then, scientists have worked to develop a cheap method to quickly and reliably sequence an individual's entire genome and have launched the international project "the 1000$ genome" (Dondorp and Wert, 2013). The project led to the appearance of the next-generation sequencing instruments.

Over the past two decades, it was shown that polymers and other analytes could be used to estimate the size of nanometer-scale features in protein ion channels for exemple, water-soluble polymers were used to physically characterize geometric featureswithin bacterial pore-foring toxins, including the dimeter, location of the

limiting aperture and pore length (Kullman et al, 2002; Purnell and Schmidt, 2009).

Recent advances suggest that these same nanometer-scale pores may become useful for the detection, identification, and characterization of a wide range of analytes, including polymers like DNA (Wang et al, 2018).

This new wave of technologies is led by Pacific Biosciences (PacBio) of Menlo Park, CA, USA and by the relative newcomer, Oxford Nanopore Technologies (ONT), of Oxford, UK. Pacific Biosystems (Norris, 2016). Both technologies analyze individual molecules of DNA with no need for artificial amplification, and generate longer reads than second-generation technologies, but both platforms have a relatively high error rate compared with Illumina's <1% error rates (Leggett and Clark,2017) .

In 2014, Oxford Nanopore Technologies (ONT) released a new third generation sequencing platform. The MinION is an USB-powered device, measuring 4 inches and weighting only 90g, commercialized together with two flowcells and reagents that cost only US$1000. ONT's technology has already begun to universalize sequencing, giving to scientists the opportunity to acquire their own sequencer and to use genomics in their research. The ONT permit sequencing of none amplified native DNA of more than 100 kbp in a short time (2-10h) with an error rate varying between 3-15%.

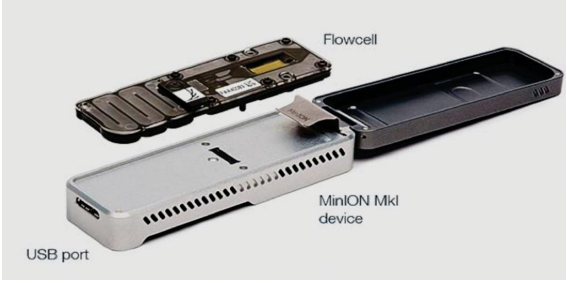


**Figure 1**: MinIon device (from oxford nanopore technologies).

Nanopore sequencing has been shown to be able to discriminate individual nucleotides by measuring the change in electrical conductivity as DNA molecules pass through the pore. The most nanopores used are made by a single ion channel formed by the *Staphylococcus aureus* endotoxin α-hemolysin (Celaya et al, 2017), or Mycobacterium smegmatis porin A (MspA). These nanopores are narrow channels of 1 nm that only single stranded DNA or RNA chains can pass through them (Duan et al, 2016). To investigate double stranded DNA chains, it was proposed recently to explore the engineered bacteriophage phi 29 protein channel. It has a larger diameter, closer to 3.6 nm and higher conductance than other biological nanopores (Wang et al, 2018a).

To replace the protein nanopores new solid-state nanaopres have been developped, they are more robust durable and mechanically more stable. However, solid-state nanopores have not yet achieved the degree of precision in analyte physical characterization that their protein counterparts have demonstrated (Kasianowicz, 2012).

## 3- Application of ONT to analyse genome of infectious agents:

The MinIon technology has been applied to sequence genome and to detect mutation in infectious microorganisms (table 1). The device has been used to analyse resistant genes of tuberculosis stains in sub Saharan Africa (Bates et al., 2016) and in diagnostic and analysis of the Ebola virus in West Africa (Kilianski et al, 2015). Another demonstration of the sequencing capabilities of MinION is provided by Quick et al, 2016 that report it uses to monitor Ebola spread, to detect mutation sub-lineages and to evaluate patient's response to vaccination. Similarly, the origin and spread of the Zika virus were analysed using the MinION sequencer in South America, the results were important for interpretation of the birth defects associated with Zika infection (Quick et al, 2017).

Besides, 6 hours sequencing run time, were sufficient to identify *E. coli* genome. Three poxviruses (cowpox, vaccinia-MVA, and vaccinia-Lister) were also identified and differentiated down to the strain level, despite over 98% identity between the vaccinia strains. The ability to differentiate strains by amplicon sequencing on the MinION was accomplished despite an observed per-base error rate of approximately 30% (Laver et al., 2015). A complete influenza virus genome was also obtained by the new sequencer and results shared greater than 99% identity with sequence data obtained from Illumina MiSeq and traditional Sanger-sequencing (Wang et al, 2015; Imai et al, 2018)

Runtuwene et al., 2018 have described the application of the portable sequencer, MinION, for genotyping nine genes causing resistance to the malaria parasite *Plasmodium falciparum*. The study concluded that MinION could generate reads with long sequences and acceptable quality with sequence accuracy was less than 90%. The ONT has also used to sequence the complete genome of *Fusobacterium nucleatum*, an oral bacteria that are associated with human pathologies as diverse as periodontitis, preterm birth, and colorectal cancer (Todd et al, 2018).

**Table 1:** application of MinIon technology for genome sequencing of some infectious agents

| Infectious agent | Sequencing | Reference |
|---|---|---|
| *Streptomyces avermitilis* | Complete genome | Laver et al, 2015 |
| *Borrelia burgdorferi* | Complete genome | Laver et al, 2015 |
| *E. coli K-12* | Complete genome | Laver et al, 2015<br>Kilianski et al, 2015 |
| *Hepatite B virus* | Complete genome | Sauvage et al, 2018 |
| *Plasmodium falciparum* | 9 genes :<br>- Mitochondrial apocytochrome B (*CYTB*)<br>- Sarcoplasmic/endoplasmic reticulum Ca2+-ATPase6 (*PfATPase6*).<br>- Multidrug resistance protein 1 (*PfMRP1*).<br>- Dihydrofolate reductase-thymidylate synthase (*PfDHFR*).<br>- Dihydropteroate synthase (*PfDHPS*)<br>- Translationally controlled tumor protein (*TCTP*).<br>- Chloroquine resistance transporter (*PfCRT*)<br>- Multidrug resistance protein 1 (*PfMDR1*)<br>- Kelch protein gene (*K13*) | Runtuwene et al, 2018 |
| *Infuenza virus* | Complete genome | Wang et al, 2015 |
| *Zika virus* | Complete genome | Quick et al, 2017 |
| *Ebola virus* | Complete genome | Hoenen, 2016 |

## 4- Application of ONT in cancer research and diagnostic:

Cancer is a heterogeneous disease that results from accumulation of mutations and epigenetic modifications in somatic cells. In last decade, researches have developed new anticancer drugs with a higher precision of molecular targeting. The cellular targets are genetically modified in cancer cells and are essential for tumor development and survival. Oncoprotein or oncogenes targets, which are mainly involved in various signaling pathways, are primarily products of gene fusions, obtained or functional mutations or overexpressed oncogenes (Ke and Shen, 2017). The use of a targeted therapy is restricted to patients whose tumor has a specific gene mutation that codes for the target. However, precision medicine aimed to identify patients most likely to benefit from treatment (Tsimberidou et al, 2014). For this reason, genomic sequencing is required nowadays to better manage patients health and targets therapies to achieve the best outcomes in the management of cancer disease. In this context, ONT technonology has been used to detect DNA structural variant of tumor suppressor genes *CDKN2A/p16* and *SMAD4/DPC4* in pancreatic cancer. Results show that nanopore sequencing can detect large deletions, translocations and inversions at dilutions as low as 1:100, with as few as 500 reads per sample (Norris et al., 2016).

De Jong et al., 2017 shows that MinION nanopore sequencing of long-range PCR amplicons is able to resolve the exon structure of whole BRCA1 transcripts. The study has identified 20 novels BRCA1 isoforms, 18 of which contained multiple individual splicing events. The study was successful in demonstrating the capability of the MinION device to characterize the exon structure of whole BRCA1 transcripts and proved that MinION technology overcomes limitations of traditional PCR-based techniques.

In lung adenocarcinoma, a number of molecular-targeting medicines are available, such as gefitinib, erlotinib and afatinib for EGFR;34 crizotinib, ceritinib and alec tinib for ALK;35 and vandetanib and cabozantini. The drug prescription requires molecular characterisation and mutation detection. The study of Suzuki et al., 2017 has reported the use of MinION to detect various types of mutations in cancer-related genes like EGFR, KRAS, NRAS and NF1 in lung cancer but regardless of the error-prone nature of the sequence data of MinION, in the case of homozygous mutant alleles, the cancerous mutations could be robustly detected.

The 2016 WHO (world health organisation) classifications of central nervous system tumors require molecular profiling for final diagnosis. Common genes that delineate this classification include IDH, 1p/19q, SHH, WNT, TP53, and RELA. To date, only few studies has been published using the MinION to support molecular diagnosis of central nervous system tumor tissue. Despite a small sample size, the study of Patel et al., 2018 demonstrated that the MinION could provide critical diagnostic information regarding SNPs (single nucleotides polymorphism), copy number variations, and methylation patterns within a single workday.

**Table 2:** some cancer related genes sequencing by Min Ion technology.

| Cancer type | Samples size/cell line | genes | Reference |
|---|---|---|---|
| Brain tumor | 28 patients | TP53, IDH1, TERT | Euskirchen *et al, 207* |
| Leukemia | 24 patients | BCR-ABL1 | Minervini, 2017 |
| Lung cancer | 8 patients | EGFR, KRAS, NRAS and NF1 | Suzuki, 2017 |
| Lang cancer | lung adenocarcinoma cell lines: PC-9, LC2/ad, PC-7, RERF-LC-Ad2, H1437, H1975, H2228, H2347, A549 and H322 | EGFR, KRAS, NRAS and NF1 | Suzuki, 2017 |
| Pancreatic cancer | PDAC cancer cell lines | CDKN2A/p16 and SMAD4/DPC4 | Norris et al, 2017 |
| Breast cancer | Human lymphoblastoid cell line | BRCA1 | De Jong et al, 2017 |

## 5- Application of ONT for HLA typing and immunogenetic clinical research:

The human genome contains many regions of high and low complexity that have relevance to an individual's health. Some of the most complex regions of the genome are those that encode the human leukocyte antigen (HLA) and KIR (Killer-cell immunoglobulin-like receptors). The nano sequencer MinION is a potential device to sequence the HLA allele's frequencies and KIR (killer-cell immunoglobulin like receptor) genes analysis (Ma et al., 2015; Ton et al., 2018). Another study realized by Liu et al, 2018 have reported the use ONT for HLA typing to assess the immunologic compatibility between organ donors and recipients, their study report that the platform's high error rate makes it challenging to type alleles with accuracy.

Likewise, Deutekom et al, 2017 have announced that the current status and data quality of MinION cannot yet be applied for routine HLA typing.

The application of MinION for sequencing ABO genes, revealed that the new sequencer can be regarded as a novel platform for high throughput ABO genotyping, very suitable in cases where serology is unavailable (Matern et al, 2017). This technology has been also applied for the studies of polymorphisms in Alzheimer related gene and the results showed that the device can detect genetic variation but the high rate of error makes polymorphism determination so difficult (Brooks et al., 2016;Ton et al., 2018).

Furthermore, the ONT long read is a promising technology that can be applied for diagnostics of rare diseases like with ataxia-pancytopenia syndrome and severe immune dysregulation (Boweden, 2019)

## 6- CONCLUSION:

Regarding the speed and the low capital cost, the ONT is a promising tool that opens new era for scientific research, molecular diagnostic and personalized medicine, especially in developing countries where access to sequencing technology is so limited. This new technology has successful applications within clinical microbiology, human genome sequencing, and cancer genotyping across multiple specialties. The MinIon device is also a new instrument that has the ability to advance our understanding of biological pathways and disease etiology.

## REFERENCES

**Bates M, Polepole P, Kapata N, Loose M., O'Grady J. 2016.** Application of highly portable MinION nanopore sequencing technology for the monitoring of nosocomial tuberculosis infection. International journal of mycobactériologie. S24.

**Boweden R., Davies RW., Heger A., et al. 2019. Sequencing of human genomes with nanopore technology.** *Nature Communications* 10: 1869.

**Brookes K, Patel T, Zapata-Erazo G, Barber I, Braae A, Clement N, Tamar Guetta-Baranes T, Chappell S. Morgan K. 2016.** Identifying Polymorphisms in the Alzheimer's Related APP Gene Using the Minion Sequencer. Next Generat Sequenc & Applic. 3:1

**Celaya, G., Perales-Calvo, J., Muga, A., Moro, F. & Rodriguez-Larrea, D. 2017.** Label-free, multiplexed, single-molecule analysis of protein–dna complexes with nanopores. *ACS nano* 11, 5815–5825.

**Chaisson M, Wilson R and Eichler E 2015.** Genetic variation and the de novo assembly of human genomes. *Nature Rev. Gen.* 16 627–640

**De Jong L, Cree1 S, Lattimore1 V, Wiggins G.A.R, Spurdle A S. 2017.** Nanopore sequencing of full-length BRCA1 mRNA transcripts reveals co-occurrence of known exon skipping events. Breast Cancer Research. 19:127.

***Deutekom HW., Kooter P., Greerligs J., et al. 2017.*** *P177 NGS typing results using oxford nanopore sequencing: Can minion data be reliably used for HLA typing***?** Human Immunology. *(78)* supplement :*190*

**Dondorp WJ and Wert MWR. 2013.** The 'thousand-dollar genome': an ethical exploration. *European Journal of Human Genetics*. 21: S6–S26

**Duan J., Zhuo S., Yao FJ., Zhang YN., Kan XF. 2016.** A Single-molecule Mycobacterium Smegmatis Porin A Protein Nanopore Sensor for Host-Guest Chemistry.

*Chinese Journal of Analytical Chemistry*. 44(12) : 1801-1807.

**Euskirchen P, Bielle F, Labreche K, Kloosterman WP, Rosenberg S, Daniau M, *et al.* 2017.** Same-day genomic and epigenomic diagnosis of brain tumors using real-time nanopore sequencing. *Acta Neuropathol.* 134:691-703.

**Hoenen T. 2016.** Sequencing of Ebola Virus Genomes Using Nanopore Technology. Bio Protoc. 5; 6(21): . doi:10.21769/BioProtoc.

**Imai K. , Tamura K., Tanigaki T., Mari Takizawa M., et al. 2018.** Whole Genome Sequencing of Influenza A and B Viruses With the MinION Sequencer in the Clinical Setting: A Pilot Study. *Front Microbiol*. 9: 2748

**Kasianowicz J., Reiner JE , Robertson JWF, Henrickson SE, Rodrigues C, Krasilnikov OV. 2012.** Detecting and Characterizing Individual Molecules with Single Nanopores in *Nanopore-Based Technology in **Methods in Molecular Biologie.*** Edited by Maria E. Gracheva, Springer edition. Pp264.

***Ke and Shen, 2017**. Molecular targeted therapy of cancer: The progress and future prospect.* Frontiers in Laboratory Medicine. *1(2): 69-75*

**Kilianski A, Haas JL, Corriveau EJ, Alvin T Liem AT, Willis KL, Kadavy DR, Rosenzweig CN and Minot SS. 2015**. Bacterial and viral identification and differentiation by amplicon sequencing on the MinION nanopore sequencer *GigaScience*. 4:12

**Kullman L., Winterhalter M., Bezrukov SM. 2002.** Transport of maltodextrins through maltoporin: a single-channel study. *Biophys J*. 82:803–812

**Laver T, Harrison J, O'Neill PA, Moore K, Farbos A, Paszkiewicz K, Studholme DJ. 2015**. Assessing the performance of the Oxford Nanopore Technologies MinION. Biomolecular Detection and Quantification 3: 1–8

**Leggett RM., Clark MD. 2017.** A world of opportunities with nanopore sequencing. *Journal of Experimental Botany*. 68 (20): 5419–5429.

**Liu C., Xiao F., Hoisington-Lopez J., Lang K., Quenzel P., Duffy B., Mitra RD.** 2018. Accurate Typing of Human Leukocyte Antigen Class I Genes by Oxford Nanopore Sequencing. *J Mol Diagn.* 20(4):428-435.

**Ma Y, Shi N, Li M, Chen F, Niu H. 2015.** Applications of Next-generation Sequencing in Systemic Autoimmune Diseases. Genomics Proteomics Bioinformatics. 13: 242–249

**Matern B., Groenewe M., Slangen T., .Tilanus MG. vooter C. 2017.** P095 ABO blood group typing with the Oxford nanopore minion. Human Immunology. 78 : *Supplement* : 112

**Nerbert DW and Zhang G. 2019.** Pharmacogenomics in Emery and Rimoin's Principles and Practice of Medical Genetics and Genomics. 7th edition. Academic press edition. Pp 572**.**

**Minervini CF, Cumbo C, Orsini P, Anelli L, Zagaria A, Impera L, *et al.* 2017.** Mutational analysis in BCR-ABL1 positive leukemia by deep sequencing based on nanopore MinION technology. Exp MolPathol. 103:33-7.

**Norris AL., Workman REW., Fan Y, Eshleman JR., Timp W. 2016**. Nanopore sequencing detects structural variants in cancer. Cancer Biology & Therapy. 2016, vol. 17, no. 3, 246–253

**Ozsolak F. 2012**. Third Generation Sequencing Techniques and Applications to Drug Discovery. Expert Opin Drug Discov. 7(3): 231–243.

**Patel A, Belykh E, Miller EJ, George LL, Martirosyan NL, Byvaltsev VA. 2018.** MinION rapid sequencing: Review of potential applications in neurosurgery. Surg Neurol Int. 9:157.

**Purnell RF and Schmidt JJ. 2009.** Discrimination of single base substitutions in a DNA strand immobilized in a biological nanopore. *ACS Nano* 3:2533–2538

**Quick J., Grubaugh ND., Pullan ST., et al. 2017.** Multiplex PCR method for MinION and Illumina sequencing of Zika and other virus genomes directly from clinical samples .*Nature Protocols* volume 12, pages 1261–1276

**Quick J., Loman NJ., Duraffour et al., 2016**. Real-time, portable genome sequencing for Ebola surveillance. *Nature*. 530 (11) : 228–232.

**Runtuwene LJ, Tuda JSB, Mongan AE, Makalowski W, Martin C. Frith MC, Imwong M, Srisutham S, Nguyen Thi LA, Nguyen Tuan N, Eshita Y, Maeda R, Yamagishi J. Suzuki Y. 2018.** Nanopore sequencing of drugresistance-associated genes in malaria parasites, *Plasmodium falciparum.* SCienTiFiC REPORTS. *8:8286*

**Sauvage V, Boizeau L, Candotti D, Vandenbogaert M, Servant-Delmas A, Caro V, et al. 2018.** Early MinION™ nanopore single-molecule sequencing technology enables the characterization of hepatitis B virus genetic complexity in clinical samples. PLoS ONE 13(3): e0194366. https://doi.org/10.1371/journal.pone.0194366

**Steinbock LJ., Radenovic A. 2015**. The emergence of nanopores in next generation sequencing. Nanotechnology 26 (7) : 074003 (5pp)

**Suzuki A, Suzuki M, Mizushima-Sugano J, Frith MC. Makałowski W, Kohno T, Sugano S, Tsuchihara K. Suzuki Y. 2017**. Sequencing and phasing cancer mutations in lung cancers using a long-read portable sequencer. DNA Research. 24(6): 585–596

**Todd SM., Settlage RE., Lahmers KK., Slade DJ. 2018.** Fusobacterium genomics using MinION and

Illumina sequencing enables genome completion and correction. mSphere3:e00269-18.https://doi.org/10.1128/mSphere.00269-18.

**Ton KNT, Cree1 SL, Gronert-Sum SJ, Tony R. Merriman TR.Lisa K. Stamp LK and Kennedy MK. 2018.** Multiplexed Nanopore Sequencingof HLA-B Locus in Maori and Pacific Island Samples. Frontiers in Genetics. 9:152.

**Tsimberidou AM., Eggermont AM., Schilsky RL. 2014.** Precision cancer medicine: the future is now, only better. *Am Soc Clin Oncol Educ Book.* 2014:61-9. doi: 10.14694/EdBook_AM.2014.34.61

**Wang H, Ettedgui J, Forstater J, Robertson JWF, Reiner JE, Zhang H, Chen S, Kasianowicz JJ. 2018a.** Determining the Physical Properties of Molecules with Nanometer-Scale Pores. ACS Sens. 23;3(2):251-263

**Wang S., Zhao Z., Haque F., Guo P. 2018.** Engineering of protein nanopores for sequencing, chemical or protein sensing and disease diagnosis. *Current Opinion in Biotechnology*. (51):80-89.

**Wang J., Moore NE., Deng YM., Eccles DA., Hall RJ. 2015**. MinION nanopore sequencing of an influenza genome. Front Microbiol. 6: 766.

**Wang Y , Yang O., Wang Z. 2015.** The evolution of nanopore sequencing. 449:1-21.

**Xing Ke and Lisong Shen. 2017.** Molecular targeted therapy of cancer: The progress and future prospect. *Frontiers in Laboratory Medicine*. 1 :(2):69-75.

# LUMINESCENT COMPOSITES ON THE BASE OF MICROCRYSTALLINE CELLULOSE: SYNTHESIS, FABRICATION AND PROPERTIES

*Submited on 21/02/2019 – Accepted on 03/06/2019*

**Abstract**

The data on preparation, structure and morphology of cellulose-based composites, those have oxide component as filler are reported. It is shown that depending on raw materials origin and processing degree cellulose samples reveal various degree of crystallinity (in the range 64 – 77 %). Obtained composites reveal even lesser crystallinity degree ≈ 57%. Detailed analysis of surface morphology was performed with using of scanning electronic microscopy. It was found the studied samples contains plates with sizes ~ 20 – 50 μ those consist of close-packed grains of 5-10 μ size. In the case of composites some oxide nanoparticles (sizes up to 200 nm) were incorporated into grains of microcrystalline cellulose. It was established the luminescence properties of cellulose are dependent on type of plant raw materials as well as on processing methods. These factors have influence on luminescence intensity but profile of photoluminescence bands remains practically unchanged. Under excitation in 337-532 nm spectral region the composites that contain K2Eu(PO4)(MoO4) and LaVO4:Sm are characterized by intensive visible photoluminescence. Spectra of these PL depend on excitation wavelength.

***Keywords*** **:** microcrystalline cellulose ; composite ; oxide nanoparticles ; luminescence; dilatometry.

**Y. NAOUI** [1]
**S.G. NEDILKO** [2]
**O.M. ALEKSEEV** [2]
**YU.E. GRABOVSKYI** [2]
**E.O. REZNICHENKO** [2]
**V.P. SCHERBATSKYI** [2]
**V.A. BARBASH** [3]
**O.V. YASCHENKO** [3]
**V.V. BOYKO** [4]
**V.P. CHORNII** [4]
**M.S. NEDIELKO** [5]
**T. DORBANI** [1]
**S. HAMAMDA** [1]

1 Laboratory TTSM, Frères Mentouri University Constantine, Algeria.
2 Taras Shevchenko National University of Kyiv. Kyiv, Ukraine.
3 National Technical University of Ukraine "Igor Sikorsky Kyiv Polytechnic Institute", Kyiv, Ukraine.
4 National University of Life and Environmental Sciences of Ukraine, Kyiv, Ukraine.
5 Paton Electric Welding Institute of NAS of Ukraine, Kyiv, Ukraine

## INTRODUCTION

Cellulose, as one of the most common natural polymers on Earth, is widely used for the production of functional, and among them, nanocomposite photovoltaic materials and devices based on them. In particular, it can be sensors, drives, devices for flexible electronics, etc. [1 - 4]. However, cellulose and materials on its basis are not often used or studied as optical systems or systems where optical phenomena can be inquired. Up today, known examples of such applications are evidence of the promise of this development and applications direction. This applies, e.g, to the development of solar radiation dosimeters based on the composite structure consisting of an organic dye, titanium oxide (TiO2), as a photocatalyst, and a polyvinyl-pyrrolidone as a binding agent. These components are applied to the cellulose matrix (paper) by printing. Under influence of light, due to the photocatalytic reaction of titanium oxide, which is proportional to the duration of exposure and depending on the wavelength of light, there is a loss of color density of the dye. The level of color loss can be controlled on the eye, or instrumentally, by measuring the light coefficient reflection in ultraviolet (UV) or visible bands of solar radiation [5]. Cellulose fibers containing specific luminescent compounds can be effective modifiers for textile products, papers on paper and plastic. The essential advantage of oxide luminescent compounds as modifiers is their stability and the fact that it is difficult to remove them from the cellulosic fiber even using a special treatment [6-8].

The aim of the work is to develop micro/nanostructured composites based on microcrystalline cellulose (MCC) as matrix and some complex oxides as fillers, and to find out their structural and luminescent characteristics, which should confirm the perspectives of their practical application.

In this work, we give data on the procedure of synthesis, manufacturing and structural and optical (luminescent) characterization of cellulose and MCC, synthesized in laboratory conditions at the Department of Ecology and Technology of Plant Polymers Igor Sikorsky "KPI" University. These data are compared with the similar characteristics of commercial MCC and composite materials made on its basis by cold pressing [9, 10].

To achieve the goal of work it was necessary to solve a number of problems, namely: to make samples of MCC from different representatives of domestic plant raw materials and to study their structural, morphological characteristics and physical properties; to make composite structures on the basis of the MCC and complex oxides; to study their structure and morphology; to study the

correlation between structural, morphological characteristics and physical properties of composites.

## II. MATERIALS AND METHODS OF STUDY :

Several series of samples were investigated in this work. The A series, consisting of 5 specimens (A1, A2, … , A5), is a powdered material derived from a single plant material, the hemp fibers, at various stages of the synthesis procedure of the MCC. The B series, consisting of six samples (B1, B2, ... , B6), is an MCC, made from different representatives of domestic plants: flax fibers, Hemp, Kenafu, Straw Stems, Corn and Miskanthus. The method for the MCC obtaining samples is described in [11]. The commercial MCC tablets manufactured by ANCYR-B (Ukraine) were used as starting material for the production of C and D series samples of the samples. At first, the MCC tablets were spiked and dispersed using a rotary-planetary mill. Further, the identical parts of the resulting powder, weighing ~ 0.5 g, were mixed with a certain amount of pre-prepared oxide powder. Composite samples in the C series contained the nitrate agent, $AgNO_3$. The design of the "MCC + AgNO3" composite, where $AgNO_3$ was in amount 30 mg, is hereinafter referred to as C / Ag. The procedure for making samples of the D series was somewhat different from the previous one. Here a mixture of dispersed MCC and oxide was dissolved in 50 ml of high purity ethanol and subjected to ultrasound treatment (frequency, f = 4.2 kHz, processing time, t = 20 minutes). Then, the resulting suspension was kept for 30 minutes, the liquid merged and removed sediment filtered through a filter paper and dried in atmospheric environment at temperature of 60 C. Powders of mixtures of all series were compressed into tablets in the form of a disk with a diameter of ~ 10 mm and a thickness of ~ 1 mm. The samples of A and B series were obtained at a pressure of $1.8\times10^4$ kPa/m$^2$, and samples of A and D series - under pressure of 580 kPa/m$^2$. The samples made of dispersed MCCs that do not contain oxide are designated as O/0, and all others: D/ Name of the appropriate oxide/Oxide content in mg.

The wide range of non-destructive solid-state control methods was used for research, namely, X-ray diffraction analysis, optical and electron microscopy, luminescent spectroscopy and light reflection spectroscopy. The surface morphology of the manufactured samples was investigated using an optical microscope OLYMPUS GX51. A detailed view of the samples surface was obtained using Tescan Mira 3LMU electronic beam scanning electron microscope (SEM). During measurements the diameter of the beam was 20 nm. Chemical elements microanalysis was performed using the instrumental tools of the same electron microscope. X-ray diffraction analysis of the structure of the samples structure (XRD) was performed using a powder diffractometer DRON-3M, working in Bragg-Brentano (θ/2θ) geometry and equipped with an X-ray tube BSV-28 (wavelength $\lambda_{rad}$ = 1.54178 Å). The X-ray scattering spectra were recorded in the range of 10-70° 2θ angles at the 0.1° step. Characteristics of luminescent radiation and luminescence excitation spectra were investigated in UV and visible ranges of light using the laser-spectral complexes LSK-1 and LSK-2. With these complexes, the luminescent properties can be investigated in the wavelength range of excitation, $\lambda_{ex}$, 225 - 800 nm, and in the range of wavelengths of the radiation registration, $\lambda_{reg}$, 300 - 1200 nm.

## III. RESULTS AND DISCUSSION

### *A. Analysis of Optical and Electron Microscopy Data :*

Optical microscopic images show that the surface and, apparently, the volume of samples, as "pure" - without oxides, and incorporated by them, are rather heterogeneous.

The different brightness of the image parts indicates that they are plates (plateau), located at different depths and under slightly different angles to the surface (Fig. 1 left part). A detailed analysis of the surface performed by SEM shows that these plates have a size ~ 20 - 50 microns, and they themselves consist of tightly packed grains in the size of 5 - 10 microns. The said plateau can in some cases be separated by noticeable cracks (Fig. 1 right part). In addition to the details described, it's easy to see the inclusion of another type - they have excellent color, shape and size. Obviously, these inclusions are particles of oxide compounds embedded into the matrix of the MCC. The size of the particles lies between 10 - 200 nm. We also see that oxide nanoparticles are capable of, partially agglomerating in grain size 2 - 10 microns. Observed features of morphology of samples allow us to qualify the structure of pressed samples as similar to ceramic [9].

### *B. Qualitative and quantitative analysis of the manufactured samples composition:*

The analysis of the manufactured samples composition was performed in different zones of the investigated samples. Some of them in Fig. 1b is marked with colored rectangles 1 - 3. It is not surprising that the average content of carbon atoms, C, and oxygen, O, for all samples in the zones of the above plates (zone 1) is 74-76 and 23-25%, respectively. These data confirm the above conclusion that observed in SEM images plates are the blocks of the matrix of the MCC.

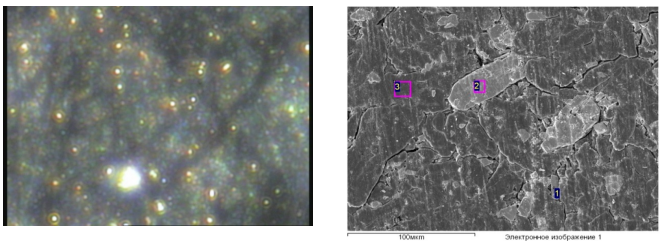


**Fig. 1.** Optical (left) and SEM (right) images of the D/$K_2Eu(PO_4)(MoO_4)$/100 sample

The analysis of the mentioned inclusions (grains and their agglomerates) in composite samples showed that they really belong to the corresponding oxides, because their composition corresponds to the chemical composition of the oxides used [9].

### C. XRD data analysis :

X-ray diffraction spectra of the MCC investigated samples in the range of 10 - 45° 2θ angles demonstrate a series of diffraction lines associated with the diffraction of X-rays on the cellulose matrix. These relatively broad lines are approximately located at 2θ angles 16; 22.5 and 34.5°. For all samples, lines and shoulders of lower intensity are also observed (Fig. 2).

There are additional lines for composite samples. Their set, position and intensity distribution correspond to X-ray diffraction spectra of oxide compounds incorporated into composites. As the content of oxides increases, the intensity of these lines increases. Thus, it can be argued that these lines correspond to the inclusion of micro/nanoparticles of oxides to the cellulosic matrix, which is confirmed by comparison of these lines characteristics (position and intensity distribution) with the corresponding characteristics for $AgNO_3$, $La_{1-x}RE_xVO_4$ and $K_2Eu(PO_4)(MoO_4)$ compounds [9]. The diffraction spectra of the of the MCC matrix both by the number of lines, their position and intensity distribution are similar for all investigated samples - "pure" and those containing oxide. At the same time, more detailed analysis shows some differences. So, firstly, the half-width of the lines is somewhat dependent on the origin of the samples: laboratory (series A and B) or commercial (series C and D), including the presence of oxide (series C and D) in their composition. These facts mean that as a procedure for removing the crystalline phase of cellulose from the starting material, which is different for laboratory and commercial specimens, and the type of oxide and its amount in the matrix, affect the distribution of nanosized MCC particles by size.

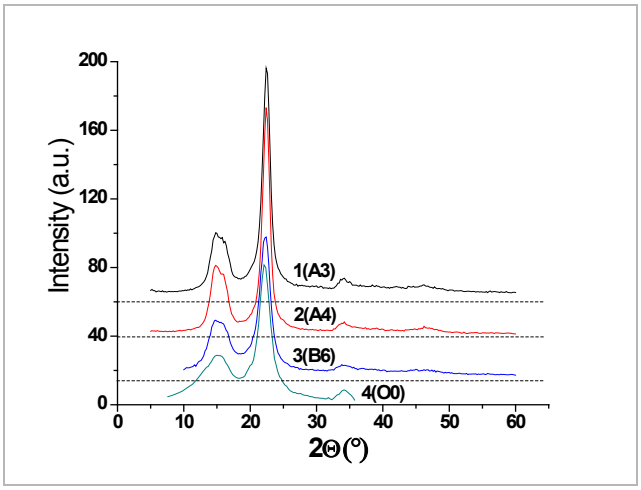


**Fig 2** : X-ray diffraction spectra for samples of different stages of MCC preparation (1, 2) and for finished MCC (3, 4); 3 - laboratory, 4 - commercial MCC. (The sample number in the series is shown in the picture).

On the basis of the measured X-ray diffraction spectra, we also estimated the crystallinity of the samples *k*, which characterizes the relative content of the crystalline phase in the investigated material. For this, the contribution of the amorphous phase ($I_{am}$) has been removed from the general spectrum: ($I_{cryst}$ + $I_{am}$). Here $I_{cr}$ is the area in the spectrum under the lines corresponding to the diffraction on the crystalline structure of the cellulose matrix, and $I_{am}$ is the area of the continuous background on which the lines are located, and this background is due to scattering on the amorphous composite material. The method of the crystalline and amorphous component in the scattering spectra separating is shown in Fig. 2. (Details of this procedure can be found in [9].) Thus, the degree of crystallinity k was estimated by the formula:

$$\kappa = \frac{I_{cr}}{I_{cr} + I_{am}} \qquad (1)$$

Calculated values fall within the limits of 64-77 % and 61-66 % for "pure" samples of laboratory and commercial MCC, respectively, whereas for composites the values of crystallinity k are significantly lower and make up 57 - 58%. Thus, the data on crystallinity indicate, firstly, the influence of the MCC synthesis procedure on the distribution of the crystalline and amorphous phases of cellulose in the finished product - MCC, and secondly, they show the influence of oxide particles on the structure and morphology of the crystalline phase of the MCC. The role of oxide micro/nanoparticles, obviously, is manifested in some destruction of the cellulose crystal lattice.

### D. Dilatometric behavior of the MCC and composites.

Discussing the results of dilatometric behavior of the samples under study ($\Delta L/L_0$ dependences, where $\Delta L = L(T) - L_0$ is the change of the sample size after heating from starting $T_0$ temperature to temperature T), it is easy to observe similar variation in dimension for the all composite samples, while $\Delta L/L_0$ behavior of the “pure” sample differs radically. Moreover, variations of the $\Delta L/L_0$ values are in the same range, despite of different behavior of corresponding $\Delta L/L_0$ curves. This range is near 13-23 $10^{-3}$, while $\Delta L/L_0$ reaches value of 40 $10^{-3}$ for the sample of minimal amount of oxide component (Fig. 3).

The description made above coincides with the data about coefficient of thermal expansions, α(T). We have found that α(T) values varies differently with temperature and the difference in variation is significant for the “pure” sample and “MCC-oxide” composites. The hidden peak of the α(T) curve is below of 40 °C and two strong dilatometric singularities are near 70 and 90 °C for the “pure” sample. Similar three features form α(T) curve for the sample of lowest oxide amount, we suppose, but they are smeared and shifted to the high temperature side, if compare with “pure” sample. (Their possible positions are near 35, 80, and 100 °C.) When oxide amount increases, only one singularity is seen near 92 and 97 °C on the α(T)

curves (Fig. 4). Described peculiarities imply that the mentioned "pure" and composite samples are strongly different. This fact is related with impact of oxide particles on the structure, morphology and size of the cellulose matrix.

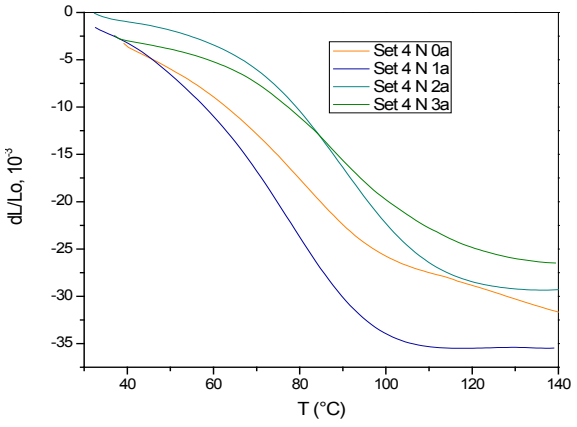


(a)

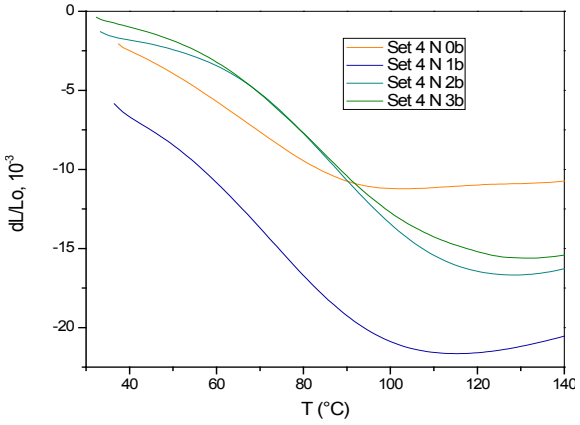


(b)

**Fig. 3**. dL/L for samples of different stages of MCC preparation (1, 2) and for finished MCC (3, 4); 3 - laboratory, 4 - commercial MCC. (The sample number in the series is shown in the picture).

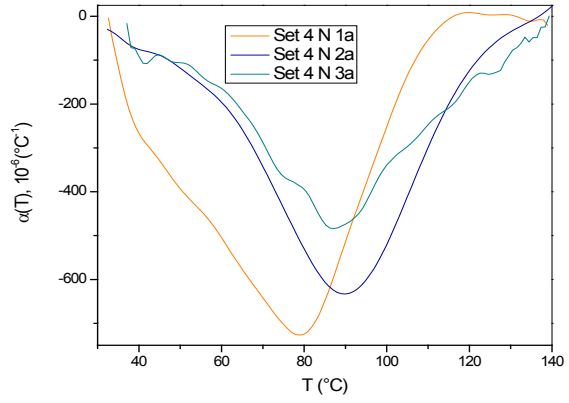


(a)

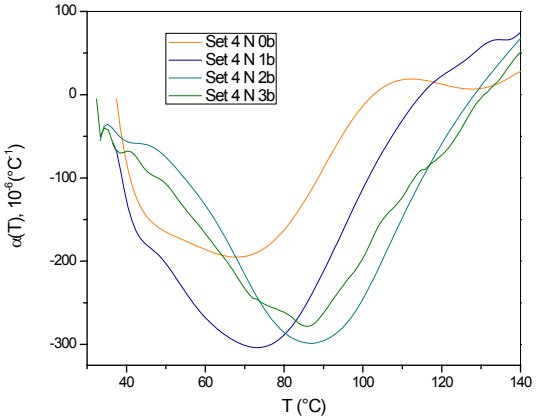


(b)

**Fig. 4**. Coefficient of dilatation for samples of different stages of MCC preparation (1, 2) and for finished MCC (3, 4); 3 - laboratory, 4 - commercial MCC. (The sample number in the series is shown in the picture).

### *E. Fluorescent properties of MCC and composites:*

A wide structural band is observed in the PL spectra of MCC produced by us at UV and violet light excitation ($\lambda_{ex}$ = 325-450 nm) regardless of MCC origin and pre-history. In the range of visible light, in this band, at least three rather intensive components that lie within the limits of 375-500, 450-550, 525-625 and 625-725 nm (can be distinguished (Fig. 5). The most intensive is the component of blue-green radiation, 450-550 nm, within which lies the maximum of the spectral band of PL, $\lambda_{max}$ = ~ 490 nm, at its excitation with $\lambda_{ex}$ = 405 nm. The PL spectra of the samples at the stages of MCC preparation and spectra of the "pure" MCC show that the pre-history of the samples and therefore their composition, structure and morphology are in some way reflected in the characteristics of the luminescence. The oxide filler also plays some role and the difference of curve 5 in Fig. 3, which corresponds to the radiation of the "MCC+ $AgNO_3$" composite, from the spectra of pure" MCC (Fig. 5, curves 3, 4) confirms that.

Therefore, we have the opportunity to assert that the observed radiation is associated with luminescent processes in the MCC matrix itself. Unfortunately, the question of their origin and the role of specific molecular components of the MCC or its derivatives (for example, carbonyl groups) is not fully understood. At the same time, the role in the luminescent processes of some molecular radicals, for example, hydroxyl groups, located on the surface of cellulose fibers, has previously been discussed.

The MCC+oxide" composites " in the case when the oxide compound in its composition contains luminescent active centers such as ions of rare earth elements ($Eu^{3+}$, $Sm^{3+}$, etc.), are characterized by bright luminescence when excited by UV or visible radiation. The PL spectra of such composite samples essentially depend on the

wavelength of excitation (Fig. 6). Thus, the blue-green radiation which is characteristic for the above-described emission of the cellulose matrix, dominates in the PL spectra at short-wave excitation ($\lambda_{ex}$ = 325 - 405 nm).

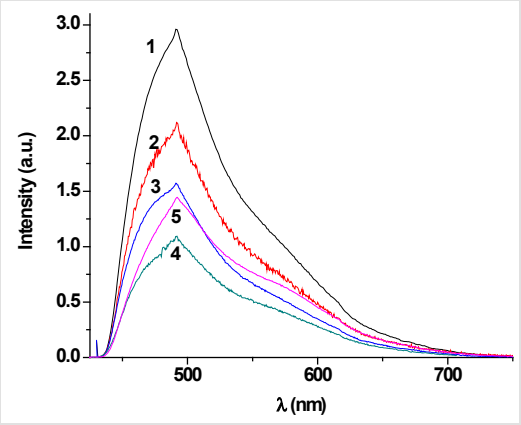


**Fig.5**. The PL spectra of the samples: A2 (1), A3 (2), A5 (3), B6 (4), and C/$AgNO_3$ composite (5)

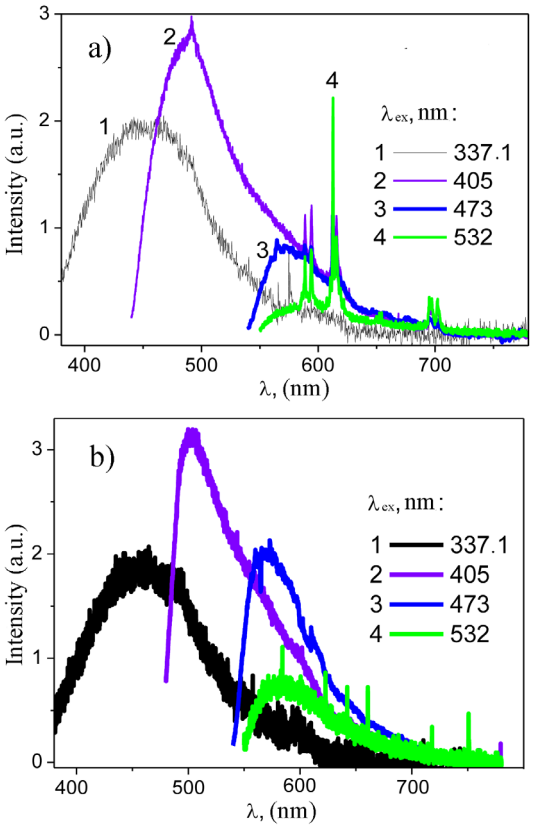


Fig. 6. The PL spectra of the composites D/K2Bi(PO4)(MoO4):Eu/100 (a) and D/$LaVO_4$:Sm:Eu/10 (b); the wavelength of excitation is indicated in the Figure; T = 300 K.

The use of longer-wave excitation leads to an increase in the intensity of the long-wave components of the PL and the displacement of the maximum of the PL band to the long-wavelength side of the spectrum and to the appearance of line spectra which is characteristic of rear - earth ions, $Eu^{3+}$ and Samarium, $Sm^{3+}$, in solid-state matrices [9].

## IV. CONCLUSIONS

1. Composite samples made by cold pressing method, where microcrystalline cellulose (MCC) is a matrix and the complex oxide compounds $AgNO_3$, $LaVO_4$: Sm, Eu and $K_2Bi$ $(PO_4)(MoO_4)$:Eu are the fillers, have a ceramic-like structure formed by the MCC plates and oxide grains.

2. The composites are characterized by intense photoluminescence in visible light, whose spectrum consists of a wide band of luminescence of the cellulose matrix and a set of narrow lines caused by the emission of ions of rare-earth elements: $Eu^{3+}$ and samarium, $Sm^{3+}$.

3. Taken results are the basis for further development of the studied cellulose-oxide composites as violet and blue light luminescent transformers and followed creation on their basis of new type of the "white" light emitting diodes.

## REFERENCES

[1] W.W. Tassi, G Nancy, Z. Hongl, "Nanocellulose-based translucent diffuser for optoelectronic device applications with dramatic improvement of light coupling," Applied materials and interfaces, vol. 7, pp. 26860 - 26864, 2015.

[2] X Wang, K.Z. Gao, Z.Q. Shao, X.Q. Peng, X. Wu, F.J. Wang, "Layer-by-layer assembled hybrid multilayer thin film electrodes based on transparent cellulose nanofibres paper for flexible supercapacitors applications," J. Power Sources, vol. 245 pp.148–155, 2014.

[3] A.C.M. Moraes, P.F. Andrade, A.F. Faria, M.B. Simoes, F.C.C.S. Salomao, E.B. Barros, M.D. Goncalves, O.L. Alves, "Fabrication of transparent and ultraviolet shielding composite films based on graphene oxide and cellulose acetate," Carbohydr. Polym., vol. 123, pp. 217–227, 2015.

[4] H.Z. Song, L.W. Zheng, "Nanocomposte films based on cellulose reinforced with nano-$SiO_2$: microstructure, hydrophilicity, thermal stability, and mechanical properties," Cellulose, vol. 20, pp. 1737–1746, 2013.

[5] P.S. Khiabani, A.H. Soeriyadi, P.J. Reece, J.J. Gooding, "Paper-Based Sensor for Monitoring Sun Exposure," ACS Sens., vol 1, pp. 775−780, 2016.

[6] Yu Bian, Beihai He, Junrong Li, "Preparation of cellulose-based fluorescent materials using Zinc sulphide quantum dot-decorated graphene by a one-step hydrothermal method," Cellulose, vol. 23, pp. 2363-2373, 2016.

[7] P. Kulpinski, A. Erdman, T. Grzyb, S. Lis, "Luminescent cellulose fibers modified with cerium fluoride doped with terbium particles." Polymer composites, vol 37, pp. 153-160, 2016.

[8] T.G. Rials, W.G. Glasser, "Thermal and dynamic mechanical properties of hydroxypropyl cellulose Films," J. Appl. Polym. Science., vol. 36, pp.749-758, 1988.

[9] M. Nedielko, S. Hamamda, O. Alekseev, V. Chornii, M. Dashevskii, M. Lazarenko, K. Kovalov, S.G. Nedilko, S. Tkachov, S. Revo, V. Scherbatskyi, "Mechanical, dielectric, and spectroscopic characteristics of "micro/nanocellulose + oxide" composites," Nanoscale Research Letters, vol. 12, pp. 98, 2017.

[10] V.A. Barbash, M.G. Karakutsa., I.V. Trembus, O.V. Yaschenko, "Development of technology of microcrystalline cellulose from hemp fibres," Eastern-European J. of Enterprise Tech., vol. 3/6, pp. 51-56, 2016.

[11] V.A. Barbash, Yu.M. Nagorna, "Technology of the microcrystalline cellulose production from non-wood vegetable raw materials (in Ukrainian)," Naukovi visti NTU "KPI"», vol 2, pp. 119-124, 2015.

# THEORETICAL STUDY OF CATHODOLUMINESCENCE OF CdTe INFLUENCE OF BULK PARAMETERS.

*Submited on 11/02/2018 – Accepted on 13/04/2018*

**Abstract**

The effect of bulk parameters (¬diffusion length (Ln), absorption coefficient (α) and acceptor concentration (Na)) on the cathodoluminescence intensity (ICl) of p type CdTe has been theoretically investigated. To do this a self-consistent calculation method of (ICl) has been used. The obtained results show that ICl decreases when Ln and α increase up to a certain excitation energy E0, and then begins to decrease. The maximum of the ICl = f(E0) curves shifts towards high energies.

***Keywords:*** *Cadmium Telluride, Cathodoluminescence, Bulk parameters, Self consistent method.*

**D. KENIECHE**

Laboratory of Physics and Chemistry of Semiconductors, Physics Department, Faculty of Exact Sciences, Frères Mentouri University Constantine, Algeria.

## I. INTRODUCTION

The use of the scanning electron microscopy in cathodoluminescence mode (SEM-CL) has a great merit for the investigation of materials at a microscopic scale.

The cathodoluminescence (Cl) is a very powerful technique which allows a spatial and spectral characterization of semiconductors. It has been widely used for the determination of parameters such as the diffusion length of the minority carriers, the absorption coefficient and the surface recombination velocity [1-7].

However, a determination, as accurate as possible, of these parameters needs an exact description of the Cl signal generation.

Until now, little attention has been paid to the theoretical study of the cathodoluminescence on cadmium telluride, as well as, the Cl dependence with the material parameters is much less developed.

In addition, there is no detailed theoretical information and also no results available on the influence of the bulk parameters on Cl.

Most previous theoretical studies of the Cl relate to the case of GaAs [8, 9]. That is why this work is of particular importance.

The study is based on a theoretical model allowing the calculation of the Cl intensity [10,11], in order to investigate the influence of bulk parameters (diffusion length, absorption coefficient and doping concentration) of the material, on Cl signal.

The role of these parameters has been determined through the discussion of the curve profiles of the signal versus the beam acceleration energy.

## 2. THE THEORETICAL MODEL

The modeling of cathodoluminescence phenomena and the approximations used are based on the following assumptions:

- The studied sample is CdTe p type: it is considered semi-infinite, homogeneous, and divided on two regions, the depletion region (at the surface) and the neutral region (in the volume).

- It is assumed that there is no radiative recombination in the depletion region, and that the electron-hole pairs generated by the incident electron beam, normal to the surface, are separated on two opposite directions due to the existence of the electric field [8].
- The capture coefficient of electrons and holes is the same.
- The defects considered are surface defects. They have: an energy level $E_t$, a concentration $N_t$ and a charge Q.
- A self-consistent method has been used for the calculation of the thickness $Z_d$.

- In the neutral region, we assume that the defects don't affect the minority carrier concentration.

- The minority carriers, generated by the electron beam (characterized by the current intensity $I_p$ and the incident energy $E_0$) have steady-state diffusion.

- The analytical form of the energy dissipation function, is that proposed by Wu and Wittry [12], it is a modified Gaussian approximation, given by:

$$\phi(u) = A.\exp\left[-\left(\frac{u-u_0}{\Delta u}\right)^2\right] - B\exp\left(-\frac{bu}{u_0}\right) \qquad (1)$$

$\Delta u$, $u_0$, b, B/A are constants, given in the case of CdTe by the following values [11]:

$\Delta u = 0.17$, $u_0 = 0.057$, $b = 3$, $B/A = 0.5$

u is the normalized penetration ($u=\rho.z/R_e$), ρ the density of the material (in $g/cm^3$ ) and $R_e$ the maximum penetration

depth of electron, given by K. Kanaya and S. Okayama [13]:

$$\mathrm{Re}(\mu m) = 0.0276 \frac{A}{\rho Z^{0.889}} E_0^{1.67} \qquad (2)$$

Where A is the atomic weight ($A_{CdTe}$ = 240), Z the atomic number ($Z_{CdTe}$ = 50), $E_0$ being the incident energy in keV, ρ the density of the material ($\rho_{CdTe}$ = 6.1g/cm$^3$).

## 3. RESOLUTION OF THE CONTINUITY EQUATION

To calculate the signal Cl, we have to resolve the continuity equation (3) of a steady-state on one dimension, which is the depth z in the neutral region.

$$div.\vec{J}_n = G_n(z) - R_n(z) \qquad (3)$$

Where $G_n(z)$ and $R_n$ (z) are the generation and recombination rates of minority carriers, respectively, $\vec{J}_n$ the flux of the minority carriers, due to the diffusion component (gradient of concentration) only. $\vec{J}_n$ is given by:

$$\vec{J}_n = -D_n \, grad(\Delta n) \qquad (4)$$

Where $D_n$ is the coefficient of diffusion.
For the low injection case, for a p-type semiconductor (Δp and Δn << $p_0$), the recombination rate will be given by:

$$R_n = \frac{\Delta n(z)}{\tau_n} \qquad (5)$$

Where $\tau_n$ is the electron lifetime, related to the diffusion length $L_n$ and the diffusion coefficient $D_n$ by: $\tau_n = \frac{L_n^2}{D_n}$

The relationship between the generation rate and the function of the dissipation energy ϕ (u) is given by:

$$G(z) = \frac{\rho}{R_e}\phi(u) \qquad (6)$$

Taking into account the equations 4 and 5, the continuity equation can be rewritten as follows:

$$-D_n \frac{d^2\Delta n(z)}{dz^2} = G - \frac{\Delta n(z)}{\tau_n} \qquad (7)$$

The solution of this differential equation is:

$$\Delta n(z) = B_n \exp\left[-\frac{(z - Z_d)}{L_n}\right] + \frac{L_n}{2.D_n}\int_{z_d}^{z} G(z')\left\{\exp\left(-\frac{|z - z'|}{L_n}\right) - \exp\left(-\frac{z + z' - 2Z_d}{L_n}\right)\right\}dz' \qquad (8)$$

Where $B_n$ is a constant, giving the excess electron concentration at ($Z=Z_d$: $B_n = \Delta n|_{Z=Zd}$).

## 4. CALCULATION OF THE CL SIGNAL INTENSITY

The total luminescence emitted from the sample is the intensity of the cathodoluminescence signal ($I_{Cl}$) [7].

$$I_{Cl} = (1 - R)\int_V A'(z)\ \eta.\frac{\Delta n(z)}{\tau}.dz \qquad (9)$$

Where V is the sample volume, Δn (z) the concentration of the excess minority carriers, η the luminescence efficiency coefficient, equal to $\tau/\tau_r$, τ being the total lifetime given by: $1/\tau = 1/\tau_r + 1/\tau_{nr}$, $\tau_r$ and $\tau_{nr}$ being the radiative and nonradiative lifetime respectively, (1-R) is the transmission coefficient through the surface and R the reflection coefficient, which can be expressed from the refractive index *n* by:

$$R = \left(\frac{n-1}{n+1}\right)^2 \qquad (10)$$

For CdTe *n* is equal to 2.75.
A' (z) is the correction function of the optical losses at the depth z given by [14]:

$$A'(z) = \int_0^{\theta_c} \exp\left(\frac{-\alpha z}{\cos\theta}\right)\sin\theta \, d\theta \qquad (11)$$

where α is the absorption coefficient, $\theta_c$ the critical angle of total reflection on the surface, which depends on the refractive index of the material, we have:
$\sin\theta_c = 1/n$ [15].

If $\theta_c$ is not high enough, as is the case for CdTe ($\theta_c$ = 21°), we can approximate the relation (11) and obtain:

$$A'(z) \approx \exp(-\alpha.z) \qquad (12)$$

The calculation of $I_{CI}$ was subject to the following approximations:

- The reflection coefficient will remain low as long as the critical angle of total reflection is low.
- The excitation by means of electron beam can be approximated by a point source situated in the volume.
- The correction function of energy losses is given by the formula 12.
- Only radiative processes in the neutral region are considered, the lifetime will be $\tau \approx \tau_r$.
- The generation of electron-hole pairs due to the absorption of the internal luminescence is assumed to be negligible.

Taking into account these approximations, the simplified model of weak excitation conditions, in the case of the band to band energy emission, was used. Thus the total Cl intensity is given by:

$$I_{Cl} \approx \int_{Z_d}^{+\infty} \frac{\Delta n(z)}{\tau_r}\exp(-\alpha.z)dz \qquad (13)$$

## 5. RESULTS AND DISCUSSION

The variation of the cathodoluminescence intensity ($I_{Cl}$) with the incident electron beam energy is shown in Fig.1. These curves are the best ones providing quantitative results.

The influence of $L_n$, $\alpha$ and Na parameters will be discussed in detail later in this work. The influence of the diffusion length can be seen on fig.1: for a given value of $L_n$, $I_{Cl}$ increases until a maximum, reached for a certain value $E_0$, that moves significantly to high energies when $L_n$ increases.

Generally $I_{Cl}$ decreases with increasing $L_n$, due to the excess carriers, which take a long time for recombination.

The appearance of a maximum for all the three values of $L_n$ is related, on one hand, to carriers recombination, which generate the Cl signal, and on the other hand, to the optical absorption of the material, which reduces the Cl intensity. We are in the presence of competition between two phenomena: the minority carriers recombination is dominant up to a maximum, reached for some value $E_0$, and then the optical absorption of the material becomes predominant. In addition, a shift of the maxima towards high energies is observed. It is explained, once again, in terms of recombination time: as soon as the $L_n$ increases the time becomes longer and we need, therefore, more energy.

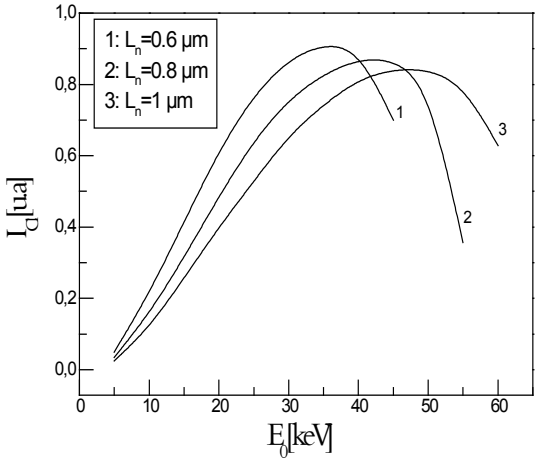


**Figure 1.** Variation of $I_{Cl}$ intensity as a function of incident energy for different diffusion lengths. ($I_p=10^{-10}$A, $E_t$=1.3eV, $N_t=10^8$cm$^{-2}$, $N_a=10^{15}$cm$^{-3}$, $\alpha=10^4$cm$^{-1}$).

The absorption coefficient, as shown in Fig. 2, acts significantly on Cl. This latter decreases with increasing absorption coefficient. Generalizing, we can say that $I_{Cl}$ would vanish for high values of $\alpha$. Every curve has a maximum for a certain $E_0$, which shifts, weakly, towards high energies. This shift is explained in terms of diminution of $\alpha$ effect at high energies: the absorption is delayed in comparison with lower energies.

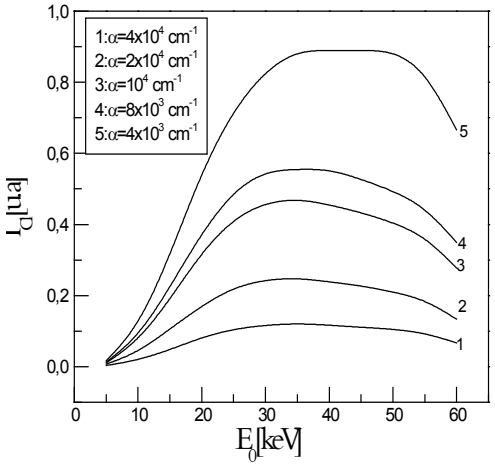


**Figure 2.** Variation of $I_{Cl}$ intensity as a function of incident energy for different absorption coefficients. ($I_p=10^{-10}$A, $E_t$=1.3eV, $L_n$=1µm, $N_t=10^8$cm$^{-2}$, $N_a=10^{15}$cm$^{-3}$).

Figure 3 shows the influence of the doping concentration on $I_{Cl}$. We note that $I_{Cl}$ decreases with increasing $N_a$ up to a well determined value of incident beam energy. This can be explained by the rate of nonradiative recombination, which increases when $N_a$ increases if we are in the low injection case. For high energies, the phenomenon is reversed because we are in high injection case. This explains why the curves and their maxima, of course, are shifted towards high energies.

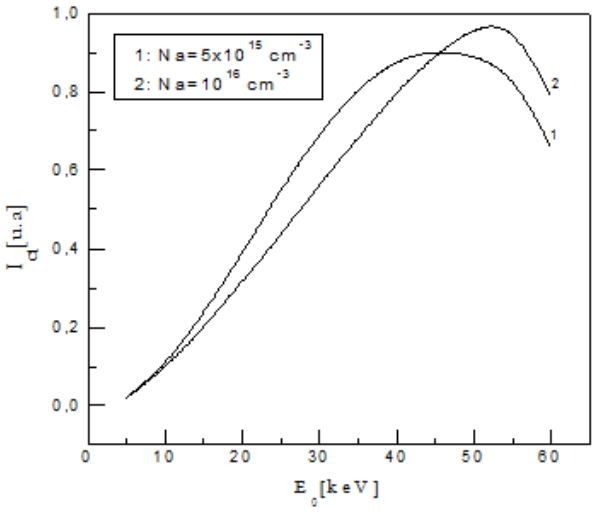


**Figure 3**. Variation of $I_{Cl}$ intensity as a function of incident energy for different doping concentrations. ($I_p=10^{-10}$A, $L_n$=1µm, $E_t$=1.3eV, $N_t=10^8$cm$^{-2}$, $\alpha=10^4$cm$^{-1}$).

## 6. CONCLUSION

In this study the influence of the most important bulk parameters (diffusion length ($L_n$), absorption coefficient ($\alpha$) and acceptors concentration ( $N_a$)) on the cathodoluminescence intensity ( $I_{Cl}$) of p type CdTe has been theoretically demonstrated.

All curves show the same behavior, and each has a maximum, due to two competing phenomena, the first is the generation-recombination of electron-hole pairs, which increases the luminescence and dominates at low energies, the second is the absorption, which contributes to the decrease in luminescence, in particular, for high energy.

The obtained results indicate that the Cl makes a difference between the volume and surface phenomena: the influence of L, $\alpha$ and $N_a$ parameters is more significant (great difference between the curves) for high energies, while for low energies this influence is weak.

By adjusting the theoretical and experimental curves quantitative values of the various parameters can be estimated.

The accuracy of the results led us to propose the model used in this study to predict experimental results by choosing the best conditions.

## ACKNOWLEDGEMENTS

I would like to thank Professor K. Guergouri for his help and advice.

## REFERENCES

[1] N. L. Dmitruk, V. G. Litovchenko and G. H. Talat, The effect of the surface space charge region on the cathodoluminescence of semiconductors, *Surface Science* 72, (1978), 321-341.

[2] W. Hergert, P. Reck, L. Pasemann, and J. Schreiber, Cathodoluminescence measurements using the scanning electron microscope for the determination of semiconductors parameters, *Phys. Stat. Sol. a* 101, (1987), 611-618.

[3] C. H. Jacob Phang, K. L. Pey and S. H. Daniel Chan, A simulation Model for cathodoluminescence in the Scanning Electron Microscope, *IEEE Transactions on Electron Devices* 39, (1992),782-791.

[4] D. B. Wittry, D. E. Kyser, Measurement of diffusion lengths in direct-gap semiconductors by electron beam excitation, *J. Appl. Phys*. 38, (1967), 375-382.

[5] V.M. Leonov, A .G.Molchanov, Y.M. Popov and G.H. Talat, Investigation of the influence of surface annihilation of excitons on cathodoluminescence of CdS, *Sov. Phys. Semicond.* 10, (1976), 852-855.

[6] T. I. Kovtunuva, N.N. Mikheev, A. N. Polyakov, and M. A. Stepovich, On the possibility of the mathematical modeling of the dependence of cathodoluminescence intensity on the energy of beam electrons with the use of the power series approximation in the problem of identifying the parameters of semiconductor meterials, *J. Surf. Inv. X-ray, Sync. Neut. Tech.* 4, (2010), 778-783.

[7] F. Cléton, B. Sieber, R. A. Masut, L. Isnard, J. M. Bonard and J. D. Ganière, Photon recycling as the dominant process of luminescence generation in an electron beam excited n-InP epilayer grown on an $n^+$-InP substrate, *Semicond. Sci. Technol.* 11, (1996), 726-734.

[8] A. Djemel, R.J.Tarento, J. Castaing, Y. Marfaing and A. Nouiri, Study of electronic surface properties of GaAs in cathodoluminescence experiments, *Phys. Stat. Sol. (a)*, 168, (1998) 425-430.

[9] A. Djemel, A. Nouiri, S. Kouissa, and R. J. Tarrento, Cathodoluminescence calculation of GaAs. Surface analysis and comparison, *Phys. Stat. Sol. (a)*, 191, (2002), 223-229.

[10] D. Kenieche and K.Guergouri, Theoretical calculation of cathodoluminescence: Infuence of surface and bulk parameters on the depletion region of p-type CdTe, *Mod. Phys. Lett. B* , 30, (2016),1650057.

[11] D. Kenieche and K. Guergouri, Theoretical Investigation of the Effect of the Surface Parameters on Cathodoluminescence Signal, *J. Mat. Sci. Eng*., 5, (2011), 473-477.

[12] C. J. Wu, D.B. Wittry, Investigation of minority-carrier diffusion lengths by electron bombardment of schottky barriers, *J. Appl. Phys.,* 49, (1978), 2827-2836.

[13] K. Kanaya , S. Okayama, Penetration and energy-loss theory of electrons in solid targets, *J. Phys. D : Appl. Phys*., 5, (1972),43-58,.

[14] W. Hergert and L. Pesemann, Theoretical study of the information depth of the cathodoluminescence signal in semiconductor materials, *Phys. Stat. Sol. a* 85, (1984), 641-648.

[15] B. G. Yacobi et D. B. Holt, *Cathodoluminescence Microscopy of Inorganic Solids*, Ed. Pelenum Press, New York and London, (1990), 68.

# A BAYESIAN PREDICTIVE PROCEDURE FOR TWO STEPS EXPERIMENTAL TRIALS.

*Submited on 25/10/2016 – Accepted on 05/05/2019*

**Abstract**

Bayesian predictive procedures give the researcher a very appealing method to evaluate the chances that the experiment will end up showing a conclusive result, or on the contrary an inconclusive one. The prediction can be explicitly based on either the hypothesis used to monitor the experiment expressed either in terms of prior distribution, on partially available data, or on both. In this paper, we propose a Bayesian predictive methodology based on two steps which can be used to develop an adaptive design for the experimental trials. This procedure does not require intensive computation and comprehensive simulations. We have used the non-informative prior to give evidence on the objectivity of the experimental data.

***Keywords:*** *Bayesian prediction, p-value, clinical trials, Monte-Carlo simulations, exponential models, stopping rule.*

***MSC2010:*** *62K05*

**Z. DJERIDI** [1]

**H. MERABET** [2]

1 Mathematics Department, Jijel University, Jijel, Algéria.

2 Laboratory of Applied Mathematics and Modeling, Mathematics Department, Frères Mentouri University Constantine, Algeria.

## INTRODUCTION

The Bayesian approach brings a major flexibility to the statistical methodology of the experimental trials. A major strength of the Bayesian paradigm is the ease with which one can make predictions about future observations. In particular, we are interested in using this approach aiming at prediction in the context of experimental trials. The role which the predictive probability plays in the design and monitoring trials is important in several fields (reliability of systems medicine, biology, ecology,...) ([18], [9]).

Bayesian predictive procedures have made an important contribution to inference and data analysis. Within this perspective, Bayesian predictive probabilities are a particularly useful device to communicate with the investigator. They give them a very appealing method to answer essential questions such as: "Given the current data, what is the chance that the final result will be in some sense conclusive, or on the contrary inconclusive? This question is unconditional because it requires consideration of all possible values of parameters. Whereas, traditional frequentist practice does not address these questions, predictive probabilities give them direct and natural answers. In particular, predictive procedures can be used to illustrate the effects of planning an experiment with a very small sample size, and to aid in the decision to abandon an experiment early.

For example, in phase II cancer trials, it is undesirable to stop a study early when the test drug is promising, and it is desirable to terminate the study as early as possible when the test treatment is not effective due to ethical consideration. For this purpose, a multiple stage design single arm trial is often employed to determine whether the test treatment is promising for further testing ([5]; [3]; [8]).

The methodology adapted to the context of clinical trials is characterized by many constraints and unsatisfactions and forms the subject of a deep and continuous development ([13]; [2]; [10]; [8]). One of the reasons for such interest is likely to emanate from the fact that public health authorities are responsible for the permission of putting the drugs into market and they play a primordial role in the elaboration of a rigorous methodology of clinical trials, taking into consideration the views of all the actors in this field (industries, public institutes of research, hospitals and scientific journals).

The primary goal clinical trial is to evaluate the efficiency and the tolerance of a new medical treatment. They are characterized by complex actions that cannot be readily modeled and they do not depend solely on statistical considerations (see for example [3]). In this situation, we, often, get primary experimental information in the form of step I, then we need to confirm some results ([3]; [8]; [9]). Formally, we consider the following situation: Using the data of the first sample, we can plan an experiment (a new sample) in a way to have good chances to get the intended conclusion if the experimentation is not discarded.

The main objective of this paper is to provide a hybrid Bayesian-frequentist procedure for two stages designs to test the efficacy of a new therapy. This procedure is based on the concept of the index of satisfaction which is a decreasing function of the p-value, and we envisage, given the available data, to calculate a predicted satisfaction of this index by considering the previous observations using Bayesian approach. Many authors have advocate to use Indexes in such situation as Lecoutre et al:1995, Merabet ,2004, Merabet and Labdaoui, 2015, Djeridi and Merabet, 2015, ([13][15][16][6]) because of their simplicity and flexibility in measuring the degree of satisfaction in the case of obtaining a significant result. We used this index to find a stopping rule for designing a phase II clinical trials. In this situation, we are led to a Bayesian approach butl with a frequentist test in mind.

Bayesian posterior probability, which is the probability that the parameter is contained within a meaningful region, is the best tool to answer the following question addressed by interim monitoring:" Is there convincing evidence in favor of the null alternative hypothesis?" On the other way, using stochastic curtailment methods such as, predictive probability and prediction of satisfaction, we give answers to the question: "Is the trial likely to show convincing evidence in favor of the alternative hypothesis if additional data are collected?" Because we deal, here, with the prediction of what evidence will be available at later stages in the study ([18]). If the futility is defined as a trial being unlikely to achieve its objective, then it is inherently a prediction problem and is best addressed using prediction of satisfaction.

To illustrate our procedure, we studied several exponential models choosing a non-informative prior to highlight the analysis objectivity of the experimental data. It is usual in experimental research to assume non-informative priors, as a study is expected to bring evidence by itself ([12]). Bayesians use at or otherwise improper non-informative priors in situations where prior knowledge is vague relative to the information in the likelihood, or in settings where we want data (and not the prior) to dominate the determination of the posterior ([13]). Furthermore, the Jeffrey's priors are a particular choice because it is an exact counterpart of the arbitrariness involved within the frequentist approach (section 2.3). The numeric calculations and the simulation results are presented in the form of binary outcomes for phase II clinical trials and Gaussian model.

## 2. STATISTIC METHODS

Bearing in mind that, that the experimental context consists of two successive experimentations, of results $\omega' \in \Omega'$ and $\omega'' \in \Omega''$, which are in general carried out independently. Their distributions built in the framework of a well established model, depend on a parameter $\theta \in \Theta$, only $\omega$" is used to found the official conclusion of the study and to determine the user's satisfaction denoted $\phi(\omega")$ (and on the choice of the decreasing function L about which we will come back in 2.4). But, on the basis of the result $\omega'$ of first step clinical trial, it is useful to anticipate what the satisfaction will be after the second step. In our study, this prediction is carried out in a Bayesian context, i.e., based on the choice of a prior probability on $\Theta$.

We denote:

$P_\Theta$: Prior probability on $\Theta$.

$P_\Theta^{\omega'}$: P*oste*rior probability on $\Theta$, *based* on the result of the *fi*rst step.

$P_{\Omega"}^{\theta}$: Sampling distribution of the second step.

$P_{\Omega"}^{\omega'}$: Probability on $\omega$", conditioned by the result of the first step.

### *2.1* General Case:

In this experimental context, we will introduce the concept of the index of satisfaction relative to a hypothesis test where the null hypothesis is of type $\theta \leq \theta_0$, in a framework where such a test may be constructed using a reasonable test function.

Let us suppose a model $(P_\theta)_{\theta\in\Theta}$_and test a null hypothesis $\Theta_0$ versus an alternative $\Theta_1$ , defined by an application $\Psi(:\Theta \to IR)$. We suppose that a point $t_0$ exists so that:

$$\boldsymbol{\theta \in \Theta_0 <=> \Psi(\theta) \leq t_0}$$

Otherwise, let us suppose that we have a real application $\boldsymbol{\xi(\Omega" \to IR)}$ such that*:*

$$\boldsymbol{\Psi(\theta_1) < \Psi(\theta_2) => \forall t, P_{\theta_1}[\xi \leq t] \geq P_{\theta_2}[\xi \leq t]}$$

Then a test of a level $\boldsymbol{\alpha}$, of $\boldsymbol{\Theta_0}$ versus $\boldsymbol{\Theta_1}(=\{\boldsymbol{\theta};\ \boldsymbol{\Psi(\theta) > t_0}\})$ is defined by rejecting the hypothesis if the experimental result, y, verifies that $\boldsymbol{\xi(y) > g(\alpha)}$, **where** $\boldsymbol{g(\alpha)}$ is the (1-α)-quantile of the distribution of $\boldsymbol{\xi}$ when $\boldsymbol{\Psi(\theta_0) = t_0}$.

Indeed, the critical region, C, of this test, is then the set of the observations y, such that $\boldsymbol{\xi(y) > g(\alpha)}$ and because of the stochastic creasing of the distributions of ξ, we have, for all $\theta_0$ such that $\boldsymbol{\Psi(\theta_0) = t_0}$,

$$\boldsymbol{\forall \theta \in \Theta_0, P_\theta(C) \leq P_{\theta_0}(C) \leq \alpha}$$

Moreover, if $\boldsymbol{\theta_1 \in \Theta_1}$ and $\boldsymbol{\theta_2 \in \Theta_1}$ with $\boldsymbol{\Psi(\theta_1) < \Psi(\theta_2)}$,

then $\boldsymbol{P_{\theta_1}(C) \leq P_{\theta_2}(C)}$ which means that the power function increases with $\boldsymbol{\Psi(\theta)}$.

### 2.2 Advantage of the p-value

The *p-value* is a measure of statistical evidence that appears in virtually all experimental research papers. Its interpretation is made extraordinarily difficult because it is not part of any formal system of statistical inference. As a result, the *p-value*'s inferential meaning is widely and often wildly misconstrued (see for example [1]), a fact that has been pointed out in innumerable papers and books appearing since at least the 1940s. S. Goodman (2008) [7] reviewed a dozen of these common misinterpretations and explained why each is wrong. He, also, reviewed the possible consequences of these improper understandings or representations of its meaning.

The *p-value* is defined as the probability, under the assumption of no effect or no difference (the null hypothesis), of obtaining a result equal to or more extreme than what was actually observed (Fig. 1).

The curve represents the probability of every observed outcome under the null hypothesis. The *p-value* is the probability of the observed outcome $(\boldsymbol{x})$ plus all "more extreme" outcomes, represented by the shaded "tail area".

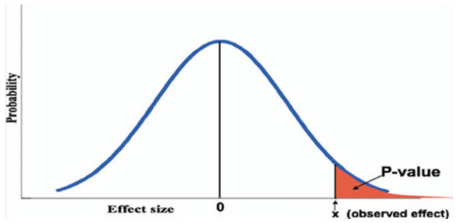


**Figure 1**: Graphical depiction of the definition of a (one-sided) *p-value*

In some cases particularly in the two sided testing problems, there are difficulties in defining a *p-value*. To eliminate these difficulties, we follow Fisher and define it as follows:

**Definition1**: The *p-value* associated with a test is the smallest significance level $\boldsymbol{\alpha}$ for which the null hypothesis is rejected. That mean, if

$$\boldsymbol{p(x) = \inf\{\alpha; x \in \Omega^{\alpha}\}}$$

Which eliminates ambiguities (as long as $\boldsymbol{\Omega^{\alpha}}$ is specified for each $\boldsymbol{\alpha}$).

**Remark 2**: According to Hwang et al. (1992) [11], the *p-value* is admissible in the one sided tests under some conditions, and it is a minimax rule under absolute error loss. They presented a number of examples in which the *p-value* is generalized Bayes, hence admissible under squared error loss function that it is a reasonable measure of accuracy. *P-values* are thus adaptive procedures that can be acceptable from a frequentist point of view (17).

### 2.3 A brief comment about the choice of the prior distribution

A prior distribution captures all of the information known about the parameters $\theta$ before we collect data.

Along with the likelihood function, it is one of the two key components of a Bayesian model.

The traditional *p-value* is based on the samples that are "more extreme" than the observed data (under the null hypothesis).

But, for discrete data, it depends on whether include the observed data or not. For instance, the usual binomial test, for example, is conservative. But if the observed data are excluded, the test becomes liberal (12). A typical solution to overcome this problem consists in considering non-informative prior distributions ([17], [9]).

These priors cannot be expected to represent exactly total ignorance about the problem at hand, but should rather be taken as reference or default priors, upon which everyone could fall back when the prior information is missing. Then, these particular prior distributions must be derived from the sample distribution, since this is the only available information.

While there are a number of formalisms for developing non-informative prior distributions, one of the most common uses Jeffreys' rule, which results in a distribution often called a Jeffreys' prior. Define the expected Fisher information as:

$$\boldsymbol{I(\theta) = -E\left[\frac{d^2 \log(f(y|\theta))}{d\theta^2}\right]}$$

Jeffreys' rule defines a non-informative prior as

$$\boldsymbol{f(\theta) = [I(\theta)]^{1/2}}$$

More fundamentally, the choice of a prior depending on Fisher information is justified by the fact that $\boldsymbol{I(\theta)}$ is widely accepted as an indicator of the amount of information brought by the model (or the observation) about $\boldsymbol{\theta}$ ([17]).

### 2.4 Index of satisfaction

This notion finds its origins in situations where the statistician, who carries out a test, "wishes" to detect a significant effect, *i.e.*, to reject the null hypothesis $\boldsymbol{H_0}$. Correspondingly, this statistician is, especially, more satisfied if, in function of the experimental results, this effect seems to be more significant.

#### 2.4.1 Rudimentary index:

Being $\boldsymbol{\alpha}$ fixed, let a test of level $\boldsymbol{\alpha}$ be defined by a critical region $\boldsymbol{\Omega_1^{"(\alpha)}}$. A first index of satisfaction is defined by:

$$\boldsymbol{\phi(\omega") = 1_{\Omega_1^{"(\alpha)}}(\omega")}$$

At a fixed $\boldsymbol{\omega'}$, the prediction is:

$$\boldsymbol{\pi(\omega') = P_{\Omega"}^{\omega'}\left(\Omega_1^{"(\alpha)}\right)}$$

$$\boldsymbol{= \int_{\Omega_1^{"(\alpha)}} P_{\Omega"}^{\theta}(\Omega_1^{"(\alpha)}) P_{\Theta}^{\omega'}(d\theta)}$$

Where $\boldsymbol{P_{\Omega"}^{\theta}(\Omega_1^{"(\alpha)})}$ is the power of the test for the value of $\boldsymbol{\theta}$.

The weakness of this index is that it expresses a satisfaction in "all or nothing" fashions (significant or not significant).

#### 2.4.2 Improved index

It is more interesting to take into account to what level will the result always appear significant. This is what the users highlight by giving, at the end of the test procedure, not only the conclusion in terms of "all nor thing" but also the smaller value of threshold for which the obtained result will be considered significant that is, from the point of view of the theory of the test, the *p-value* given in definition 1, and it is in our case

$$\boldsymbol{p = P_{\theta_0}\left(\xi > \xi(\omega'')\right)}$$

An index of satisfaction (*IS*), for the considered test of level $\boldsymbol{\alpha}$, is then defined naturally by an application from the results set in $\boldsymbol{IR_+}$ such that:

- Takes the value $\boldsymbol{0}$ if we don't reject the hypothesis, i.e., if $\boldsymbol{\xi(y) \leq g(\alpha)}$,

- And if $\boldsymbol{\xi(y) > g(\alpha)}$, is a decreasing function of $\boldsymbol{P_{\theta_0}(\xi > \xi(y))}$, which we denote

$$\boldsymbol{L(P_{\theta_0}(\xi > \xi(y)) = L(1 - F_{\theta_0}(\xi(y)))}$$

where $\boldsymbol{F_{\theta_0}}$ is the distribution of ξ at the frontier such as $\boldsymbol{\Psi(\theta_0) = t_0}$.

**Remark 3**: A rudimentary index is the indicator function of the critical region (which was studied by Grouin (1994)[13]) but it does not take into account of the "*p-value*".

### 2.5. Prediction of satisfaction

Being $\alpha$ fixed, let a test of level $\alpha$ be defined by a critical region $\Omega_1^{''(\alpha)}$. It is more interesting to take into account to what level will be the results always appear significant. We will use the new index of satisfaction (mentioned in section 2.4.2), wich was studied by Merabet H. (2004)[15], and defined for the bayesian tests, based on the same prior $P_\Theta$, as:

$$\phi(\omega'') = \begin{cases} 0 & si \quad \omega'' \in \Omega_0^{''(\alpha)} \\ 1 - inf\left\{\beta; \omega'' \in \Omega_1^{''(\beta)}\right\} & si \quad \omega'' \in \Omega_1^{''(\alpha)} \end{cases} \quad (1)$$

A standard situation is that where an application $\psi(\Theta \to \mathbb{R})$ is such as $\Theta_0 = \{\theta;\ \psi(\theta) \le t_0\}$ and where it also exists $\xi(\Omega'' \to \mathbb{R})$ and $g(]0,1[ \to \mathbb{R})$ such that

$$\Omega_1^{''(\alpha)} = \{\omega'';\ \xi(\omega'') \le g(\alpha)\}$$

Where $g(\alpha)$ is the $(1-\alpha)$ quantile of the distribution of $\xi$ when $\psi(\theta_0) = t_0$.

Using the *p-value;*

$\boldsymbol{p(\omega'') = P_{\theta_0}(\xi > \xi(\omega''))}$,

the index of satisfaction is thus defined naturally as

$$\phi(\omega'') = \begin{cases} 0 & if \quad \xi(\omega'') \le g(\alpha) \\ L(p(\omega'')) & if \quad \xi(\omega'') > g(\alpha) \end{cases} \quad (2)$$

Where $L$ is a decreasing function.

Let $F_{\theta_0}$ be the distribution of $\xi$ at the frontier, *i. e.*, for any $\theta_0$ such as $\psi(\theta_0) = t_0$, the index of satisfaction is defined by:

$$\phi(\omega'') = \begin{cases} 0 & if \quad p(\omega'') \ge 1 - \alpha \\ L\left(1 - F_{\theta_0}(\omega'')\right) & else \end{cases} \quad (2)$$

The prediction of satisfaction is then given by:

$$\boldsymbol{\pi(\omega') = \int_{\Omega_1^{''(\alpha)}} \phi(\omega'')\, P_{\Omega''}^{\omega'}(d\omega'')}$$

$$\boldsymbol{= \int_{\Theta} \left( \int_{\Omega_1^{''(\alpha)}} \phi(\omega") P_{\Omega''}^{\theta}(d\omega'') \right) P_{\Theta}^{\omega'}(d\theta)}$$

$$\boldsymbol{= \int_{\{\omega'';\xi(\omega'')>g(\alpha)\}} L\left(1 - F_{\theta_0}(\omega'')\right) P_{\Omega''}^{\omega'}(d\omega'')}$$

It is noticed that

$\int_{\Omega_1^{''(\alpha)}} \boldsymbol{\phi(\omega") P_{\Omega''}^{\theta}(d\omega'')}$ generalizes the power of the test in the logic of the index of satisfaction proposed.

We can generalize this procedure to a family of limited indexes defined by

$\boldsymbol{L(p) = (1-p)^l}$, where $\boldsymbol{l \ge 0}$.

It is preferable to choose limited indexes because they are easy to interpret.

**Remark 4:**

1. If $\boldsymbol{l = 1, 1 - \phi(\omega'')}$ is the p-value.

2. In the case where $\boldsymbol{l = 0}$, one finds the indicator function of the critical region which is the rudimentary index of Grouin ([13]).

## 3. APPLICATION

Djeridi and Merabet (2016) [6] proposed to calculate explicitly or numerically the prediction of satisfaction in several exponential models: binomial, poisson, gamma and gaussian for $L(p) = (1-p)$ in the case of a test of threshold, $\alpha$ where the null hypothesis is

$H_0: \theta \le \theta_0$. We are led to a Bayesian approach, ( but still with a frequentist test in mind) when the prior distribution of the unknown parameter $\theta$ is non-informative. In this case, we choose the *Jeffreys' prior* (section 2.3).

### 3.1 Binomial distribution

Let us suppose that all random variables are independent $X'_i\ (1 \le i \le k)$ and $X''_j\ (1 \le j \le n)$ has a bernoulli distribution $B(\theta)$, where $\theta$ is unknown.

Then $\omega' = \sum_{i=1}^{k} X'_i$ has a binomial distribution $B(k, \theta)$ and $\omega'' = \sum_{j=1}^{n} X''_j$ has a binomial distribution $B(n, \theta)$.

By choosing the non-informative prior of Jeffrey's for $\theta$:

$$f(\theta) = \theta^{-\frac{1}{2}}(1-\theta)^{-\frac{1}{2}} \propto Beta\left(\frac{1}{2}, \frac{1}{2}\right)$$

The posterior density of $\theta$ given $\omega'$ is a beta distribution $Beta\left(\omega' + \frac{1}{2}, k - \omega' + \frac{1}{2}\right)$ ([10]), and the predictive of $\omega''$ given $\omega'$ is given by:

$$\nu(\omega''|\omega') = \frac{C_n^{\omega''}\beta\left(\omega'' + \omega' + \frac{1}{2}, n + k - (\omega' + \omega'') + \frac{1}{2}\right)}{\beta\left(\omega' + \frac{1}{2}, k - \omega' + \frac{1}{2}\right)}$$

Where $\beta(x,y) = \frac{\Gamma(x)\Gamma(y)}{\Gamma(x+y)}$

$and\ C_x^y = \frac{x!}{y!(x-y)!}$.

Then, the index of satisfaction *(IS) i*s:

$$\phi(\omega'') = \begin{cases} 0 & if \quad \omega'' < q_0 \\ \sum_{t=0}^{\omega''-1} C_N^t {\theta_0}^t (1-\theta_0)^{N-t} & if\ \omega''is\ integer\ and\ \ \omega'' \geq q_0 \end{cases}$$

Where

$$q_0 = inf\left\{u; \sum_{t=u}^{N} C_N^t {\theta_0}^t (1-\theta_0)^{N-t} \leq \alpha\right\}$$

and, the prediction of satisfaction *(PIS)* is:

$$\pi(\omega') = \sum_{\omega''=q_0}^{N}\left(\sum_{t=0}^{\omega''-1} C_N^t {\theta_0}^t (1-\theta_0)^{N-t}\right)\nu(\omega''|\omega')$$

$$= \sum_{\omega''=q_0}^{N}\left(\sum_{t=0}^{\omega''-1} C_N^t {\theta_0}^t (1-\theta_0)^{N-t}\right) \times \frac{C_N^{\omega''}\beta\left(\omega'' + \omega' + \frac{1}{2}, N + K - (\omega' + \omega'') + \frac{1}{2}\right)}{\beta\left(\omega' + \frac{1}{2}, K - \omega' + \frac{1}{2}\right)}$$

### 3.2 Poisson Sampling

Let us suppose that $X'_i\ (1 \leq i \leq n)$ and $X''_j\ (1 \leq j \leq k)$ are *i.i.d.* real random variables of Poisson distribution $\mathcal{P}(\theta)$, where $\theta$ is unknown.

Then $\omega' = \sum_{i=1}^{n} X'_i$ have a Poison distribution $\mathcal{P}(n\theta)$ and $\omega'' = \sum_{j=1}^{k} X''_j$ have a Poisson distribution $B(k\theta)$. If $\theta$ has a non informative prior $f(\theta) = \theta^{-1}$

Then the posterior density of $\theta$ given $\omega'$ will be

$$f(\theta|\omega') \propto Gamma(\omega', n)$$

And the predictive of $\omega''$ given $\omega'$ is

$$\nu(\omega''|\omega') = \frac{\Gamma(\omega' + \omega'')}{\Gamma(\omega')\omega''!}\left(\frac{n}{n+k}\right)^{\omega'}\left(\frac{k}{n+k}\right)^{\omega''}$$

The index of satisfaction is then expressed as:

$$\phi(\omega'') = \begin{cases} 0 & if \quad \omega'' < q_0 \\ \sum_{s=0}^{\omega''-1} e^{-k\theta_0}\frac{(k\theta_0)}{s!} & if \quad \omega'' \geq q_0 \end{cases}$$

Where

$$q_0 = inf\left\{s; \sum_{s=0}^{u-1} e^{-k\theta_0}\frac{(k\theta_0)}{s!} \geq 1 - \alpha\right\}$$

And the prediction of satisfaction is given by:

$$\pi(\omega') = \sum_{\omega''=q_0}^{\infty}\left(\sum_{s=0}^{\omega''-1} e^{-k\theta_0}\frac{(k\theta_0)}{s!}\right)\nu(\omega''|\omega')$$

$$= \sum_{\omega''=q_0}^{\infty}\left(\sum_{s=0}^{\omega''-1} e^{-k\theta_0}\frac{(k\theta_0)}{s!}\right)\frac{\Gamma(\omega' + \omega'')}{\Gamma(\omega')\omega''!}\left(\frac{n}{n+k}\right)^{\omega'}\left(\frac{k}{n+k}\right)^{\omega''}$$

### 3.3 Gamma distribution

Let us suppose that $X'_i\ (1 \leq i \leq k)$ and $X''_j\ (1 \leq j \leq n)$ are *i.i.d.* real random variables of Gamma distribution $G(p,\theta)$ where $\theta$ is unknown and $p$ is known. Then, $\omega' = \sum_{i=1}^{k} X'_i$ have a Gamma distribution $G(kp,\theta)$ and $\omega'' = \sum_{j=1}^{n} X''_j$ have a Gamma distribution$B(np,\theta)$. Let be $K = kp$ and $N = np$.

If $\theta$ has a non informative prior $f(\theta) = \theta^{-1}$. Then the posterior density of $\theta$ given $\omega'$ will be:

$$f(\theta|\omega') \propto Gamma(K, \omega')$$

And the predictive of $\omega''$ given $\omega'$ is:

$$\nu(\omega''|\omega') = \frac{1}{\beta(N,K)}\frac{(\omega')^{N-1}(\omega')^{K}}{(\omega'' + \omega')^{N+K}}$$

The index of satisfaction is then expressed as:

$$\phi(\omega'') = \begin{cases} 0 & if \quad \omega'' < q_0 \\ F(\omega'') = \int_0^{\omega''}\frac{(\theta_0)^N}{\Gamma(N)}t^{N-1}e^{-t\theta_0}dt & if \quad \omega'' \geq q_0 \end{cases}$$

Where $F(q_0) = 1 - \alpha$.

And the prediction of satisfaction is given by:

$$\pi(\omega') = \int_{q_0}^{\infty}\left(\int_0^{\omega''}\frac{(\theta_0)^N}{\Gamma(N)}t^{N-1}e^{-t\theta_0}dt\right)\nu(\omega''|\omega'')\mathrm{d}\omega''$$

$$= \int_{q_0}^{\infty} \left( \int_0^{\omega''} \frac{(\theta_0)^N}{\Gamma(N)} t^{N-1} e^{-t\theta_0} dt \right) \frac{1}{\beta(N,K)} \frac{(\omega'')^{N-1}(\omega')^K}{(\omega''+\omega')^{N+K}} \, d\omega''$$

This can be estimated numerically.

### 3.4. Gaussian model

Relying on the Central Limit Theorem, statisticians in the first half of the nineteenth century were almost always referring to the normal distribution. There are obviously many phenomena for which a normal model is not applicable, but it is still extensively used, in particular, in econometrics and in fields where the Central Limit Theorem approximation can be justified (particle reliability, etc.). In fact, the normal approximation is often justified for asymptotic reasons (see [17]). Therefore, it is of interest to study in detail this particular distribution from a Bayesian viewpoint. The corresponding calculations of the prediction being realizable by the Monte-Carlo methods (section 4).

We perform independent observations of same normal random variable $\mathcal{N}(\theta, \sigma^2)$. In all that follows, $\Phi$ and $\varphi$ (resp. $T_{n-1}$ and $t_{n-1}$) indicates the cumulative distribution function and the density of the distribution $\mathcal{N}(0,1)$ respectively (resp. of the student distribution $\mathcal{T}_1(n-1,0,1)$ ) .

The first result; $\underline{x} = (x_1, x_2, \dots, x_n)$, is a series of $n$ observations and the second result is a series; $\underline{y} = (y_1, y_2, \dots, y_k)$.

For obvious reasons of exhaustiveness, we will base all calculations on $x = \frac{1}{n}\sum_{i=1}^{n} x_i$ and $y = \frac{1}{k}\sum_{j=1}^{k} y_j$ , of distributions $\mathcal{N}(\theta, {\sigma_1}^2)$ and $\mathcal{N}(\theta, {\sigma_2}^2)$, respectively, where ${\sigma_1}^2 = \frac{\sigma^2}{n}$ and ${\sigma_2}^2 = \frac{\sigma^2}{k}$.

We suppose here that $\sigma^2$ is unknown (so ${\sigma_1}^2$ and ${\sigma_2}^2$) (The situation where $\sigma^2$ is known was studied in [15]). We choose as a priori distribution for $(\theta, \sigma^2)$ the non-informative distribution $\pi(\theta, \sigma^2) = \frac{1}{\sigma}$ ([17]). We wish to test a null assumption of type $\theta \leq \theta_0$.

We use here a usual test ranging on $\underline{y}$, whose critical region is $]q_0, +\infty[$, where $q_0 = \theta_0 + {S'}_2 u_\alpha^+$, $u_\alpha^+$ indicating the upper $\alpha$ quantile of the standard normal distribution $\mathcal{N}(0,1)$:
$\Phi(u_\alpha^+) = 1 - \alpha$ and ${S'}_2 = \frac{S_2}{\sqrt{k}}$. The posterior density associated to the prior $\pi(\theta, \sigma^2) = \frac{1}{\sigma}$ and applied to the second phase $\underline{y} = (y_1, y_2, \dots, y_k)$ is then:

$$\theta | \sigma, y, {S_2}^2 \sim \mathcal{N}\left(y, \frac{\sigma^2}{k}\right) \text{ and}$$

$$\sigma^2 | y, {S_2}^2 \sim \mathcal{IG}\left(\frac{k-1}{2}, \frac{{S_2}^2}{2}\right)$$

Where $${S_2}^2 = \frac{1}{k}\sum_{j=1}^{k}(y_j - y)^2.$$

And the predictive density of $y$ given $x$ is given by:

$$f_x(y) = \frac{\Gamma\left(\frac{n}{2}\right)}{\sqrt{\pi}\Gamma\left(\frac{n-1}{2}\right)} \frac{1}{\frac{S_1}{\sqrt{nk}}\sqrt{n+k}} \left( \frac{\frac{(y-x)^2}{S_1^2}}{\frac{kn}{(n+k)}} + 1 \right)^{-\frac{n}{2}}$$

Where ${S_1}^2 = \frac{1}{n}\sum_{i=1}^{n}(x_i - x)^2$.

We identify a student distribution $\mathcal{T}_1\left(n-1, x, \frac{S_1}{\sqrt{nk}\sqrt{n+k}}\right)$

Finally the prevision of satisfaction is:

$$\pi(x) = \int_{q_0}^{+\infty} \Phi\left(\frac{y-\theta_0}{\frac{S_2}{\sqrt{k}}}\right) \times \frac{\Gamma\left(\frac{n}{2}\right)}{\sqrt{\pi}\Gamma\left(\frac{n-1}{2}\right)} \frac{1}{\frac{S_1}{\sqrt{nk}}\sqrt{n+k}} \left( \frac{\frac{(y-x)^2}{S_1^2}}{\frac{kn}{(n+k)}} + 1 \right)^{-\frac{n}{2}} dy$$

## 4. EXAMPLES

### 4.1 Application for binary outcomes:

We consider the design for real data, taken from the study of predictive probability approach ([14]; [3]; [20]) .

In a phase II trials, an investigator plans to enroll a maximum of $N_{max} = 40$ patients into the study. At a given time $\omega' = 16$ responses are observed in $k = 23$ patients. In the light of this result should the investigator continue the trial or stop it using the index of satisfaction *IS* and its prediction *PIS* if he enrolls all patients?

Assuming a prior distribution of $\theta$ as $Beta(1/2,1/2)$ and with the number of responses in future $n = 17$ patients, $\omega''$ follows a *beta-binomial* distribution $(17, 16.5, 7.5)$. At each possible value of $\omega'' = i$, the posterior probability of $\theta$ follows a *beta* distribution $\theta|\omega', \omega'' = i \sim Beta(\frac{1}{2} + \omega' + i, \frac{1}{2} + N_{max} - \omega'' - i)$

For this example

$$\theta|\omega' = 16, \omega'' = i \sim Beta(16.5 + i, 24.5 - i)$$

In order to use the index of satisfaction *IS* for $\theta_0 = 60\%$, we have to find $q_0 = 13$, for level of significance $\alpha =$

0.05. So the index of satisfaction *IS* and its prediction *PIS* will be **Table 1**

| $\omega''$ | $\phi(\omega'')$ | $\omega'$ | $\pi(\omega')$ |
|---|---|---|---|
| | | 13 | 0.13 |
| | | 14 | 0.21 |
| | | 15 | 0.29 |
| $< 13$ | 0 | 16 | 0.40 |
| 13 | 0.9536 | 17 | 0.52 |
| 14 | 0.9877 | 18 | 0.64 |
| 15 | 0.9979 | 19 | 0.76 |
| 16 | 0.9998 | 20 | 0.86 |
| 17 | 1.0000 | 21 | 0.93 |
| | | 22 | 0.98 |
| | | 23 | 0.997 |

**Table 1:** IS and PIS for different values of $\omega'$ and $\omega''$.

In this case, the prediction of satisfaction will be $\pi(\omega' = 16) = 0.40$ and we will reject $H_0$. This result is the same as the Simon's design ([20]) and the Predictive Probability design introduced by Lee and Liu (2008) [14] but with little satisfaction. On the other hand, if we take $\omega' = 20$, then $\pi(\omega' = 20) = 0.85$ and we should reject the null hypothesis with a great satisfaction, so we are more satisfied about the efficacy of the treatment.

### 4.1.1 PIS-procedure as a stopping rule:

This procedure can be used formally as a stopping rule for clinical trials. At interim analysis, termination occurs to reject $H_0$ if the prediction of satisfaction *PIS* at point $\theta_0$is high, formally, if it is greater than a specified constant $\gamma$between 0.5 and 1.

The specific stopping criteria are typically unique to each trial and include ethical and business considerations, such as risk/ benefit considerations, available resources, opportunity cost, and overall statistical power. In the context of interim monitoring for futility, prediction of satisfaction is naturally appealing because it directly addresses the relevant question, that is, whether a trial is likely to reach its objective if continued to the planned maximum sample size.

In our example, even if we take $\gamma \geq 0.5$, than $\pi(\omega' = 17) = 0.52$ (table 1). In this case, our satisfaction will be great and we are satisfied that our treatment is promising and we should collect more information about it. Furthermore, this non-informative prior and cut-off reserve type I error which is:

$IP(\omega' > 17|\theta_0 = 0.60) = 0.05$. In this case, the actual power of this design, for an alternative of $\theta_1$=0.80, is 0.84.

Tables 2 (a) and (b) gives the values of the prediction of satisfaction *PIS* for different values of $\theta_0, k, n, \omega'$, for $\alpha = 0.05$.

| | | $\pi(\omega')\ for$ | | | |
|---|---|---|---|---|---|
| k, n | $\omega'$ | $\theta_0 = 0.2$ | $\theta_0 = 0.4$ | $\theta_0 = 0.6$ | $\theta_0 = 0.8$ |
| 23, 17 | 1 | 0.0078 | 0.0001 | 0.0000 | 0.0000 |
| | 2 | 0.0282 | 0.0004 | 0.0000 | 0.0000 |
| | 3 | 0.0688 | 0.0017 | 0.0000 | 0.0000 |
| | 4 | 0.1332 | 0.0051 | 0.0001 | 0.0000 |
| | 5 | 0.2203 | 0.0127 | 0.0004 | 0.0000 |
| | 6 | 0.3250 | 0.0271 | 0.0012 | 0.0000 |
| | 7 | 0.4392 | 0.0517 | 0.0030 | 0.0000 |
| | 8 | 0.5539 | 0.0898 | 0.0068 | 0.0001 |
| | 9 | 0.6609 | 0.1439 | 0.0141 | 0.0002 |
| | 10 | 0.7543 | 0.2152 | 0.0271 | 0.0006 |
| | 11 | 0.8308 | 0.3025 | 0.0485 | 0.0013 |
| | 12 | 0.8897 | 0.4027 | 0.0818 | 0.0029 |
| | 13 | 0.9321 | 0.5101 | 0.1303 | 0.0062 |
| | 14 | 0.9609 | 0.6179 | 0.1968 | 0.0125 |
| | 15 | 0.9790 | 0.7191 | 0.2827 | 0.0240 |
| | 16 | 0.9896 | 0.8073 | 0.3867 | 0.0444 |
| | 17 | 0.9953 | 0.8783 | 0.5045 | 0.0788 |
| | 18 | 0.9981 | 0.9305 | 0.6282 | 0.1343 |
| | 19 | 0.9993 | 0.9651 | 0.7473 | 0.2193 |
| | 20 | 0.9998 | 0.9852 | 0.8504 | 0.3428 |
| | 21 | 1.0000 | 0.9951 | 0.9279 | 0.5096 |
| | 22 | 1.0000 | 0.9989 | 0.9757 | 0.7132 |
| | 23 | 1.0000 | 0.9999 | 0.9967 | 0.91991 |

**Table 2 (a):** *PIS* for different values of $\theta_0$.

| | | $\pi(\omega')\ for$ | | |
|---|---|---|---|---|
| k, n | $\omega'$ | $\theta_0$ =0.2 | $\theta_0$ =0.5 | $\theta_0$ =0.7 |
| 15, 20 | 1 | 0.0274 | 0.0001 | 0.0000 |
| | 2 | 0.0919 | 0.0005 | 0.0000 |
| | 3 | 0.2038 | 0.0022 | 0.0001 |
| | 4 | 0.3533 | 0.0076 | 0.0003 |
| | 5 | 0.5178 | 0.0216 | 0.0013 |
| | 6 | 0.6722 | 0.0515 | 0.0043 |
| | 7 | 0.7984 | 0.1067 | 0.0122 |
| | 8 | 0.8887 | 0.1951 | 0.0304 |
| | 9 | 0.9456 | 0.3197 | 0.0680 |
| | 10 | 0.9769 | 0.4735 | 0.1373 |
| | 11 | 0.9917 | 0.6387 | 0.2508 |
| | 12 | 0.9976 | 0.7901 | 0.4144 |
| | 13 | 0.9995 | 0.9045 | 0.6167 |
| | 14 | 0.9999 | 0.9711 | 0.8197 |
| | 15 | 1.0000 | 0.9967 | 0.9649 |

**Table 2 (b):** *PIS* for different values of $\theta_0, k, n, \omega'$, for $\alpha = 0.05$.

Larger values of $\theta_0$, for example, 80% have a slower rate of convergence to 1 than the smaller values, for example, 20% (see figure 2 (a)), because we need more arguments to reject the null hypothesis. Also, for type I error, the rejection of the null hypothesis will be hard if we increase the level of significance (figure 2 (b)).

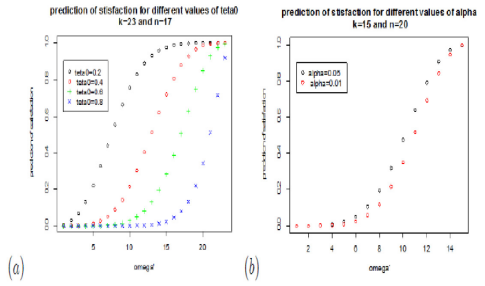


**Figure 2:** PIS augments slowly if $\theta$ increases (a) and if the level of significance is greater (b).

A criticism addressed to this procedure, that it does not give us direct Bayesian information about $\theta$ such as could provided by a credible interval. Also, to prove the efficacy of the treatment we should have a big probability of success. In the example above, the trial will stop for futility if less than 17 successes/23 (74%) are observed.

### 3.4.1. Monte Carlo's Method :

In order to carry out the calculation of $\pi(x)$ using a Monte Carlo method, and by change of variable, we rewrite it in the following form:

$$\pi(x) = [1 - T_{n-1}(a + \gamma u_\alpha^+)] \int_{-\infty}^{+\infty} \Phi\left(\frac{z - a}{\gamma}\right) \times \frac{t_{n-1}(z)}{1 - T_{n-1}(a + \gamma u_\alpha^+)} \mathbb{I}_{[a+\gamma u_\alpha^+, +\infty[} dz$$

Where $a = \frac{\sqrt{n-1}}{S'_1}(\theta_0 - x)$ , $\gamma = \sqrt{n-1}\frac{S'_2}{S'_1}$

With $S'_1 = \frac{S_1}{\sqrt{\frac{nk}{n+k}}}$, $S'_2 = \frac{S_2}{\sqrt{k}}$ , and $\frac{t_{n-1}(z)}{1-T_{n-1}(a+\gamma u_\alpha^+)} \mathbb{I}_{[a+\gamma u_\alpha^+, +\infty[}$

is the probability density $Q$ deduced from the cumulative distribution function of the student distributioned by the event $[a+, +\infty[$.

The Monte Carlo method then consists in approaching $\pi(x)$by:

$$[1 - T_{n-1}(a + \gamma u_\alpha^+)] \left[\frac{1}{N}\sum_{i=1}^{N} \Phi\left(\frac{Z_i - a}{\gamma}\right)\right]$$

Where the $Z_i$ are $N$ realisations of the probability $Q$. The pulling of the $Z_i$ proceeds in the following way:

- $U_i$ is drawn according to the uniform distribution on[0,1].
- $V_i = T_{n-1}(a + \gamma u_\alpha^+) + \left(1 - T_{n-1}(a + \gamma u_\alpha^+)\right)U_i$ ; *i.e.,* that $V_i$ follows the uniform distribution on $[T_{n-1}(a + \gamma u_\alpha^+), 1]$.

$Z_i = {T^{-1}}_{n-1}(V_i)$, *i.e.*, that $Z_i$ follows the distribution $Q$.

### 4.2. Result's representation and discussion

We will find below the representative curves of $\pi$ as a function of the observation $x = \frac{1}{n}\sum_{i=1}^{n} x_i$. We have considered only the case where $\theta_0 = 0$ and in the first as in the second sample, the observations are of the same unit variance $\sigma^2$ but where the numbers can vary, considering that a modification of $\theta_0$ and $\sigma^2$ will only result in a translation effect. We have considered, the two cases: $\alpha = 0.05$ and $\alpha = 0.01$. On the other hand, we have taken $k = 10$ , 20 or 30 for $n = 10$ (Figure 3 and Figure 4).

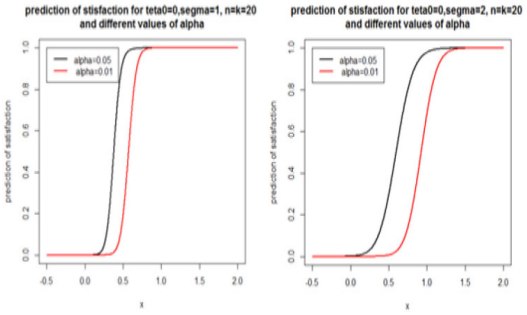


**Figure 3**: Prediction of satisfaction based on 5000 iterations for $\alpha = 0.05$, $\sigma^2 = 1$ and 4. Graphs with a step 0.001 for $x$.

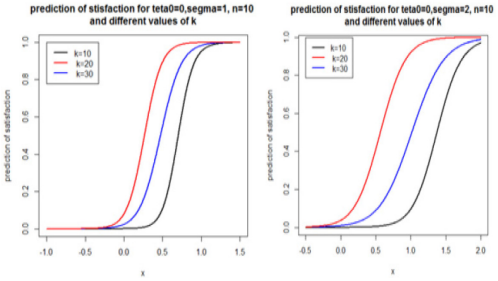


**Figure 4**: Prediction of satisfaction based on 5000 iterations for $\alpha = 0.01$, $\sigma^2 = 1$ and 4. Graphs with a step 0.001 for $x$.

Graphs (3(a)- 3(b)) represent the prediction of satisfaction when $\alpha = 0.05$. The first one is for $\sigma = 1$ and the second is for $\sigma = 2$. We see clearly that the satisfaction rises with $n$ and the convergence becomes slower in the second one and it is clear that when $k$ augments the satisfaction increases fastly.

Furthermore, graphs (4(a)- 4(b)) represent the prediction of satisfaction when $\alpha = 0.01$ and $\alpha = 0.05$ for $n = k = 10$ and $\sigma = 1$ or $\sigma = 2$ respectively. We can make the same remark but the values augment moving away from 0 fastly in the second graph than in the first one because we need more arguments to reject the null hypothesis. This conveys well the interest of the consideration of the p-value in the index of satisfaction that the reject region is more informative since $x$ is larger, which gives importance to the indicated index.

## 5. CONCLUSION

Bayesian predictive procedures have an important contribution to inference and data analysis. Within this perspective, Bayesian predictive probabilities can be used for interim monitoring of experimental trials to estimate the probability of observing a statistically significant result if the trials are to continue to its predefined maximum sample size.

The main objective of this paper is to present an answer to the question:" How to evaluate, if a given experiment will be conclusive about a hypothesis before it is performed?". The answer is given by the proposal hybrid Bayesian-frequentist procedure to evaluate whether a *p*-

*value*-based hypothesis test will yield a conclusive result in the context of clinical trials. The proposed design is based on a family of limited indexes of satisfaction which was the generalization of the "rudimentary" index of satisfaction considered in [13].

The methodology is useful in two-steps testing procedures; the result of the first step is used to decide if the experiment will be continued. Given the posterior distribution derived from the available data, the prediction of satisfaction is defined as the predictive expectation of the index of satisfaction for the future sample. We consider different cases of the application of the proposed procedure with a non-informative prior.

Furthermore, we can use this procedure to develop an adaptive design for experimental trials especially in the sequential analyses to monitor trials very well by choosing any cohort size for the steps. Examples in section 4, for both binary outcomes and it's approximation to the Gaussian model, gives the characteristics of this procedure.

For example, in the context of interim monitoring for futility for single–arm clinical trials, prediction of satisfaction is naturally appealing because it directly addresses the relevant question, that is, whether a trial is likely to reach its objective if continued to the planned maximum sample size. In this situation, the index of satisfaction can be used formally as a stopping rule. At interim analysis, termination occurs to reject $H_0$ if the prediction of satisfaction *PIS*, at a point $\theta_0$, is high, formally, if it is greater than a specified constant between 0.5 and 1. The specific stopping criteria are typically unique to each trial and include ethical and business considerations, such as risk/ benefit considerations, available resources, opportunity cost, and overall statistical power.

Bayesian experimental trial simulation is a generic tool that can compute the predictive satisfaction for any trial result, whether that is based on a Bayesian analysis of the data, frequentist significance tests or a formal decision analysis such as a decision by a health care provider to put a drug in the market. In our paper, we have taken an inferential problem related to the binary outcomes and the Gaussian model usig this methodology and this stopping rule for the trial. The simulations results have perfectly illustrated the procedure which ensures the neutrality, the objectivity and esspecially the ethical considerations. The numeric calculus were similars to those obtained by [8] and [20].

## AKNOWLEDGEMENTS

We absolutely would like to thank Mr. Zougab Nabil Professor at the University of Tizi-Ouzou and LAMOS of Bejaia, for his help and advice on the R simulation in this work. we thank too the anonymous referees for several suggestions that have improved the presentation of this paper.

## REFRENCES:

[1] Berger, J.O. and Sellke, T. (1987). Testing a Point Null Hypothesis: The Irreconcilability of P Values and Evidence.. Journal of the American Statistical Association, Vol. 82, No. 397, 112-122.

[2] Chow, S. C. (2005). Statistical consideration of adaptive methods in clinical development. Journal Biopharm. Stat., 15, 575-91.

[3] Chow, S. C., Berry, S.M., Carlin, B.P., Lee, J.J., Müller, P. (2011). Bayesian adaptive methods for clinical trials. Chapman &Hall/CRC Press, New York.

[4] Chow, S. C. Corey, R., Lin, M., (2012). On the independence of data monitoring committee in adaptive design clinical trials. Journal of biopharmaceutical statistics, 22(4): 853-867.

[5] Chow, S. C. and Chang M., (2007). Adaptive design in clinical trials. Chapman & Hall/CRC. Biostatistics Series, USA.

[6] Djeridi, Z. Merabet, H., (2016). Choice of the prior in the Bayesian design for the clinical trials . Sciences et Technologie: A , N44, 27-31.

[7] Goodman S., (2008). A Dirty Dozen: Twelve P-Value Misconceptions. In Siminar in Hematologie, 45: 135-140.

[8] Guosheng, Y. Chen, C., Lee, J.J. (2012). Phase II trial design with Bayesian adaptive randomization and predictive probability. statistical society: Series C (Applied statistics), 61, 219-235.

[9] Hamada, M. S., Wilson, A.G., Reese, C. S., Martz, H.F., (2008). Bayesian reliability. Springer Series in statistics.

[10] Hoff, P.D., (2009). A first course in Bayesian statistical Methods. Springer science + Business media, New York.

[11] Hwang, J.T., Casela, G., Robert, C., Wells, M.T., Farrell, R.H., (1992). Estimation of accuracy in testing. The annals of statistics, Vol. 20, No. 1; 490-509.

[12] Lecoutre, B, (2001). A Bayesian predictive procedures for designing and monitoring experiments. In Bayesian methods with applications to science, Policy and official statistics Luxemburg. office for official publications of the european communities, 301-310.

[13] Lecoutre, B., Derzko, G. and Grouin, J. M., (1995). Bayesian predictive approach for inference about proportions. Statistics in Medecine, 14: 1057- 1063.

[14] Lee, J.J. and Liu, D.D., (2008). A predictive probability design for phase II cancer clinical trials. Clinical Trials, 5: 93-106.

[15] Merabet, H., (2004). Index and prevision of satisfaction in exponential models for clinical trials. Statistica, anno LXIV, n3, 441-453.

[16] Merabet, H., Labdaoui, A., (2015). Bayesian prediction using two stages design in expiremental trials. Nature & Technologie A-Sciences fondamentals et engineering, n 12: 11-23.

[17] Robert, C.P., (2007). Bayesian choice.From Decision-Theoretic Foundations to Computational Implementation. Springer science + Business media, New York.

[18] Saville, B. R. , Connor, J. T. , Ayers, G. D. and Alvarez, J., (2014). The utility of Bayesian predictive probabilities for interim monitoring of clinical trials. Clin Trials,DOI: 10.1177/1740774514531352.

[19] Shao,Y., Mukhi, V., and Goldberg, J. D., (2008). A hybrid Bayesian-frequentist approach to evaluate clinical trial designs for tests of superiority and non-inferiority. Statist. Med., 27:504-519.

[20] Simon, R., (1989). Optimal two-stage design for phase II clinical trials. Controlled clinical trials, 10: 1-10.

# THE APPLICATION OF SELECTIVE HARMONIC ELIMINATION USING SIMULATED ANNEALING FOR MULTILEVEL INVERTERS.

*Submited on 07/09/2017 – Accepted on 03/06/2019*

**Abstract**

Harmonic pollution is a very common issue in the field of power electronics, Harmonics can cause multiple problems for power converters and electrical loads alike, this paper introduces a modulation method called selective harmonic elimination pulse width modulation (SHEPWM), this method allows the elimination of a specific order of harmonics and also control the amplitude of the fundamental component of the output voltage. In this work SHEPWM strategy is applied to a five level cascade inverter. The objective of this study is to demonstrate the total control provided by the SHEPWM strategy over any rank of harmonics using the simulated annealing optimization algorithm and also control the amplitude of the fundamental component at any desired value. Simulation and experimental results are presented in this work.

***Keywords:*** Multilevel inverter, harmonic elimination, simulated annealing, optimization.

**F. CHABNI**
**R. TALEB**

Laboratory of Electrical Engineering and Renewable Energies (LGEER), Electrical Engineering Department, Hassiba Benbouali University, Chlef, Algeria.

## INTRODUCTION

Electronic motor controllers play a major role in our daily life, these devices can be found anywhere especially in industrial applications. There are multiple types of power converters such as AC to DC, DC to DC and DC to AC. The Direct to Alternative Current converters (DC to AC) are the most used type of power converters for the control of alternating current motors. Cascade DC to AC multilevel inverters are suitable for high power applications they can withstand a huge amount of voltage stress; they are also very easy to make and to maintain due to their modular structure. The conventional multilevel cascade configuration can be achieved by connecting multiple H-bridge modules in series; this configuration will be briefly covered in this work. The harmonic content in an AC voltage waveform generated by an inverter can affect significantly the performance of AC machines. For example harmonics can raise the temperature of an AC motor which decreases the lifetime of the insulation and consequently the lifetime of the motor itself. One way to fight this problem is by choosing the right modulation strategy. Several modulation strategies have been proposed and studied for the control of multilevel inverters such as Sinusoidal Pulse width modulation (SPWM) [1] and space vector pulse width modulation (SVPWM) [2]. A more efficient method called selective harmonic elimination pulse width modulation (SHE-PWM) is also used; the method offers a lot of advantages such as operating the inverters switching devices at a low frequency which extends the lifetime of the switching devices. The main disadvantage of selective harmonic elimination method is that a set of non-linear equations extracted from the targeted system model must be solved to obtain the optimal switching angles to apply this strategy. Multiple computational methods have been used to calculate the optimal switching angles such as Newton-Raphson (N-R) [3], this method dependents on initial guess of the angle values in such a way that they are sufficiently close to the global minimum(desired solution). And if the chosen initial values are far from the global minimum, non-convergence can occur. Selecting a good initial angle, especially for a large number of switching angles can be very difficult. Another approach is to use optimization algorithms such as genetic algorithm (GA) [4], firefly algorithm (FFA) [5] and particle swarm optimization (PSO) [6] and differential evolution (DE) [7]. The main advantage of these methods is that they are free from the requirement of good initial guess. This article discusses the possibility of using the simulated annealing algorithm to solve the selective harmonic elimination problem, and also to demonstrate the possibility of eliminating any undesired harmonic of any rank. The simulated annealing algorithm was first introduced in 1979 by Armen G. Khachaturyan in and it was used in multiple applications such as solving facility layout problems [8], telecommunication network problems [9], optimal reactive power problem [10] and integrated circuits design [11] .In this work the SA algorithm is used to compute the optimal switching angles necessary for the SHEPWM method, in the case of a uniform step five level waveform, only one harmonic is eliminated and the fundamental component is controlled. This work is organized as follows the next section will present briefly the SHEPWM for multilevel inverters and the simulated annealing optimization method. The third section presents the obtained simulation results, simulation and experimental results are presented in the last section.

## 2. SHEPWM for multilevel inverts:

### A. Proposed converter and the SHEPWM strategy:

The structure of the converter chosen in this study is presented in left side of figure 1, the converter consists of two H-bridges , each bridge is powered by its own isolated direct current power source $V_{dc1}$ and $V_{dc2}$ with $V_{dc1}$ = 25V and $V_{dc2}$ =25V , this particular configuration can generate five voltage levels. In order to apply the SHEPWM strategy to this inverter the generated output voltage waveform has to be a simple stepped signal, the left side of Figure 1 illustrates a generalized form of a uniform stepped voltage waveform with $\theta_1$ and $\theta_2$ are the optimal angles to be computed in order to eliminate the undesired harmonics and control the fundamental component simultaneously.

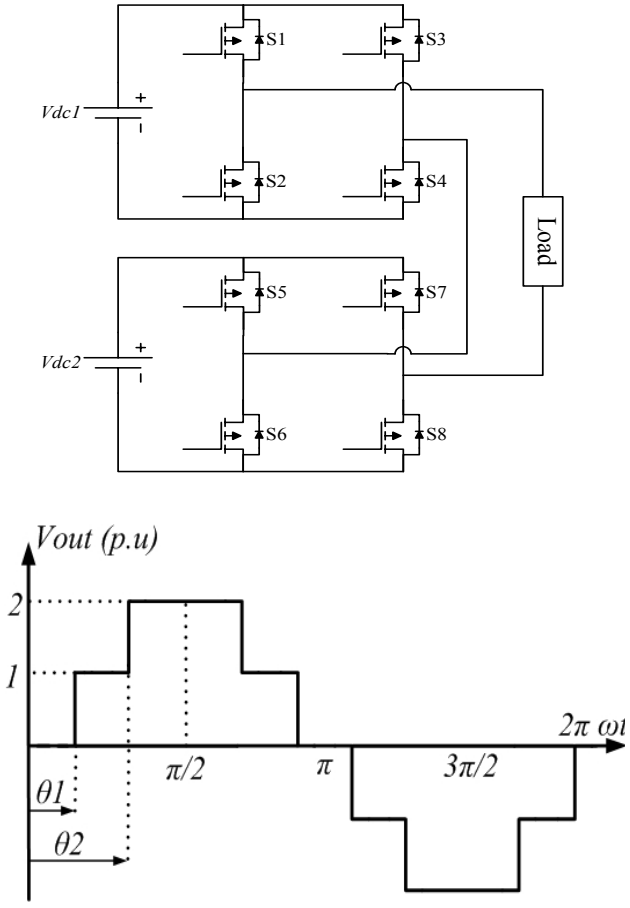


**Fig. 1.** Schematic of the proposed multilevel converter (Left) Generalized five level voltage waveform (Right)

The number of voltage levels that can be generated by Cascade multilevel inverters is generally presented by 2*P*+1 where *P* represents the number of voltage levels or switching angles in a quarter waveform of the signal, and *P*-1 is the number of undesired harmonics that can be eliminated from the generated waveform. In a five level inverter with uniform step voltage waveform, the number of voltage levels generated in quarter waveform is two plus the zero level which means only one harmonic can be eliminated. To control the peak value of the output voltage and eliminate any harmonic, with quarter and half wave symmetry characteristics of the voltage waveform are taken in consideration, the Fourier series expansion is given as:

$$V(\omega t) = \sum_{n=1,3,5,\ldots}^{\infty} \left[\frac{4V_{dc}}{n\pi}\sum_{i=1}^{p}\cos(n\theta_i)\right]\sin(n\omega t) \quad (1)$$

Where n is rank of harmonics, $n$ =1,3,5,… ,and $p$ =($N$-1)/2 is the number of switching angles per quarter waveform., and $\theta_i$ is the $i^{th}$ switching angle, and $N$ is the number of voltage levels per half waveform. The optimal switching angles $\theta_1$ and $\theta_2$ can be determined by solving the following system of non-linear equations:

$$\begin{cases} H_1 = \cos(\theta_1) + \cos(\theta_2) = M \\ H_n = \cos(n\theta_1) + \cos(n\theta_2) = 0 \end{cases} \quad (2)$$

Where $M$ = (($N$-1)/2)$r$/4), r is the modulation index and. The obtained solutions must satisfy the following constraint:

$$0 < \theta_1 < \cdots < \theta_p < \pi/2 \quad (3)$$

An objective function is necessary to perform the optimization operation, the function must be chosen in such way that allows the elimination of low order harmonics while maintaining the amplitude of the fundamental component at a desired value Therefore the objective function is defined as:

$$f(\theta_1, \theta_2) = \left(\sum_{n1}^{2}(\cos(\theta_n) - M)\right)^2 + \left(\sum_{n1}^{p}(\cos(n\theta_n))\right)^2 \quad (4)$$

The optimal switching angles are obtained by minimizing Eq (4) subject to the constraint Eq (3).The main problem is the non-linearity of the transcendental set of Eq (2), the simulated annealing is used to overcome this problem.

### B. Simulated Annealing

The simulated annealing is a stochastic global optimization method that can differentiate between multiple local optima points. The algorithm is inspired from the process of cooling metal after heating it to get a perfect crystal structure with minimum defects. While many optimization methods get stuck in a local minimum instead of converging to a global minimum, the simulated annealing solves this problem by performing a random search. Figure (2) presents a simplified flowchart of the simulated annealing algorithm.

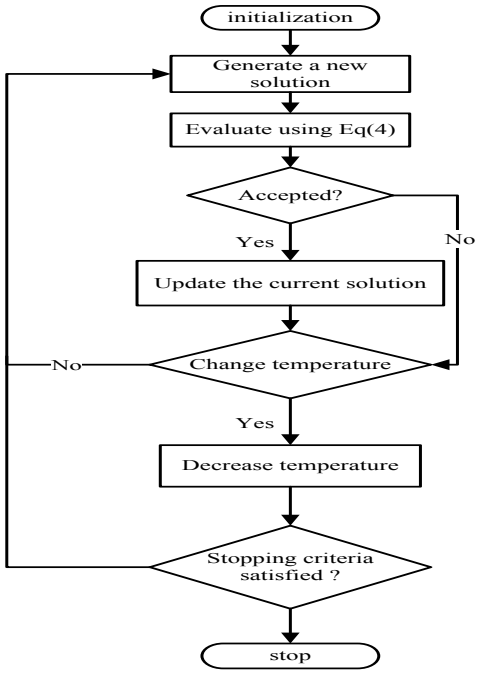


**Fig. 2.** Generalized five level voltage waveform

The algorithm deals with the minimization of an objective function using a parameter called temperature to evaluate the probability of accepting worst values to escape local minima. The algorithm starts by defining the values of parameters and algorithm operators, and also sets the temperature parameter $T$ to an initial value with initial set of solutions. In this algorithm new random solutions are generated for each iteration, if the newly generated solution improves the objective function $f(x)$ expressed in (4) and gave better result than the previous one, then the proposed solution is accepted. Another technique to evaluate the improvement of the system, is to accept the new random solution with a likelihood according to a probability of $e^{(-\Delta f)}$, where $\Delta f$ is the variation of the objective function, this variation can be expressed by the following equation.

$$\Delta f = f(x^k) - f(x^{k-1}) \qquad (5)$$

where $k$ is the current iteration.

## 3. SIMULATION RESULTS

In order to prove the theoretical predictions and to test the effectiveness of the proposed algorithm, the control method and the mathematical model of the proposed inverter were developed and simulated using MATLAB/SIMULINK scientific programming environment; the optimization program was executed on a computer with Intel(R) Core(TM) i3 CPU@ 2.13GHz Processor and 4GB of RAM, the optimization algorithm takes 127.43 seconds to complete the computation process.

The left side of figure (3), figure (4) and figure (5) show the generated waveforms in the case of eliminating the third, fifth and the seventh harmonics respectively, and for different modulation indices r where $r_1 = 0.7$, $r_2 = 0.85$ and $r_3 = 0.9$, whereas the left side of the same figures show the FFT analysis of the generated waveforms for the above mentioned cases and also for different values of r. It can be noticed from the voltage waveforms that by decreasing the modulation index, the switching angles will have higher values and this will lead to a decrease in the amplitude of the fundamental component this effect can be clearly observed in the FFT analysis figures. And also it can be clearly seen from the FFT analysis that the undesired harmonics were successfully eliminated in each case, for example in figure (3) the third harmonic was eliminated while the fifth harmonic remained untouched, whereas in figure (4) the fifth harmonic was eliminated while the third and the seventh harmonics remained untouched.

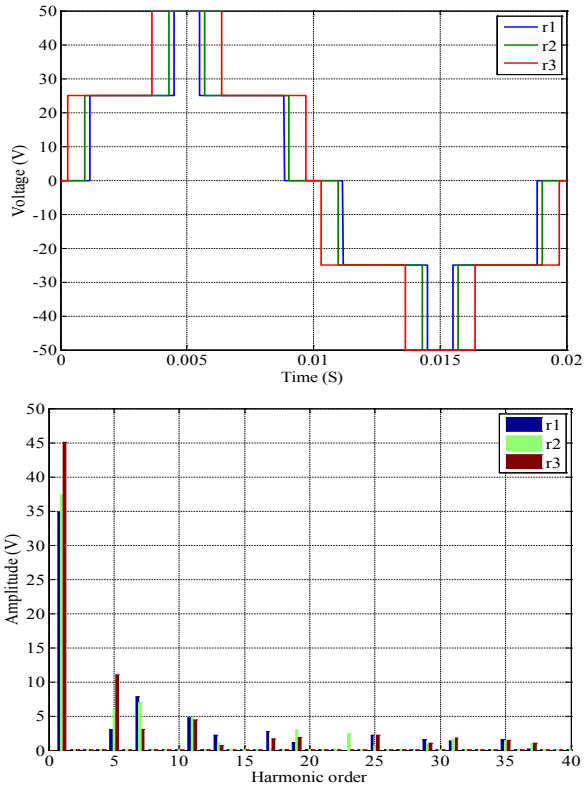


**Fig. 3.** Generated Voltage waveforms (Left) and FFT analysis (Right) in the case of eliminating the third harmonic

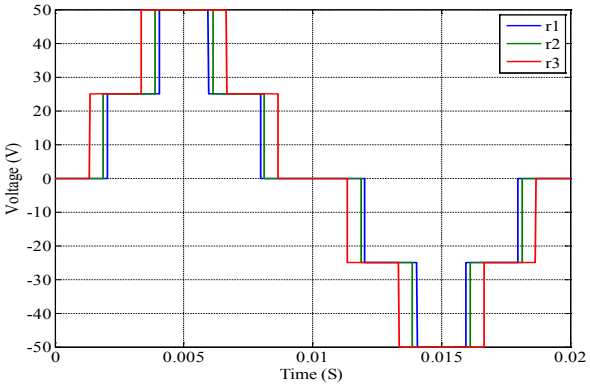

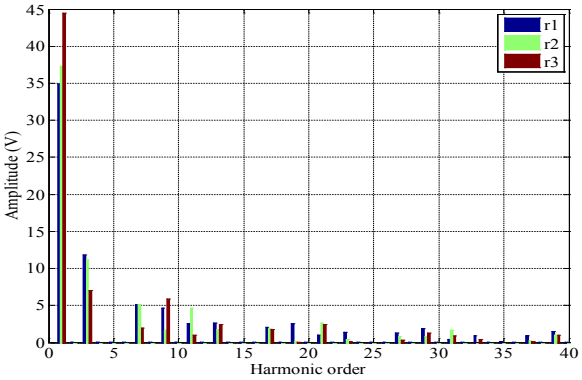


**Fig. 4.** Generated Voltage waveforms (Left) and FFT analysis (Right) in the case of eliminating the fifth harmonic

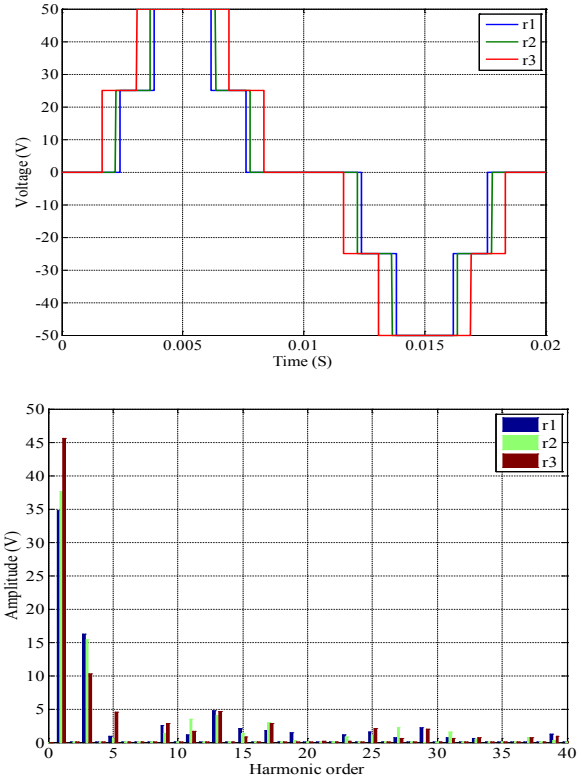


**Fig. 5.** Generated Voltage waveforms (Left) and FFT analysis (Right in the case of eliminating the seventh harmonic

## 4. Experimental results

A five level inverter prototype was built to validate the results obtained from the simulation process; Irf640 MOSFETS were used as switching devices for the proposed inverter,4N25 optocouplers were used to protect the microcontroller used in this experiment, Siglent SDS 1000 oscilloscope with FFT capability was used to preview the voltage waveforms and to perform FFT analysis. The left side figure 6, figure 7 and figure 8 show the experimental waveforms in the case of eliminating the third, fifth and seventh harmonic respectively, and each waveform was generated for a particular value of modulation index *r*. The right side of same figures show the FFT analysis of generated waveforms for the cases mentioned previously, and it can be clearly seen that the third, fifth and the seventh harmonics were successfully eliminated, and also it can be noticed that there is a slight change in the value of the fundamental component.

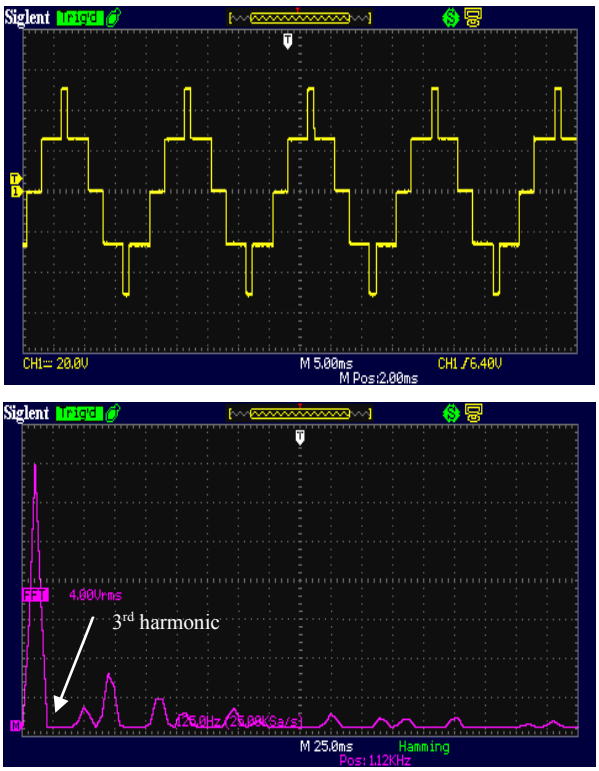


**Fig. 6.** Generated Voltage waveforms (Left) and FFT analysis (Right) in the case of eliminating the third harmonic $r = 0.7$.

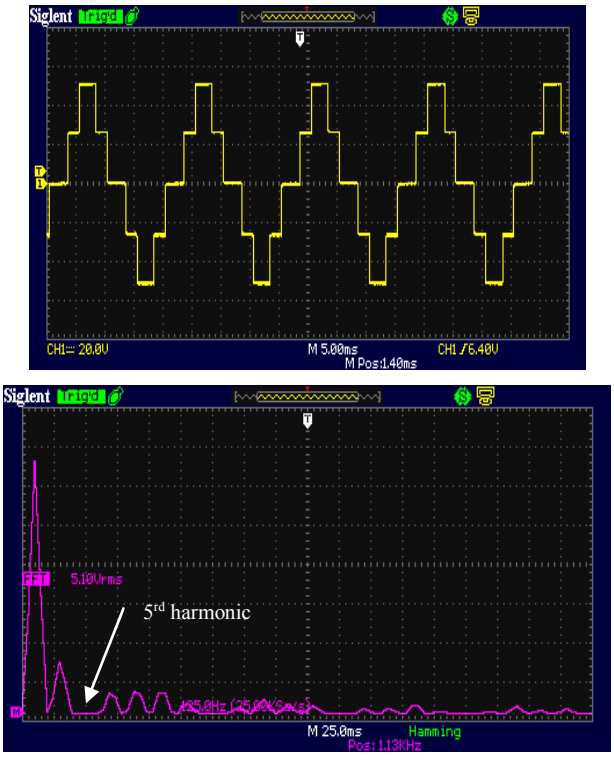


**Fig. 7.** Generated Voltage waveforms (Left) and FFT analysis (Right) in the case of eliminating the fifth harmonic $r = 0.85$.

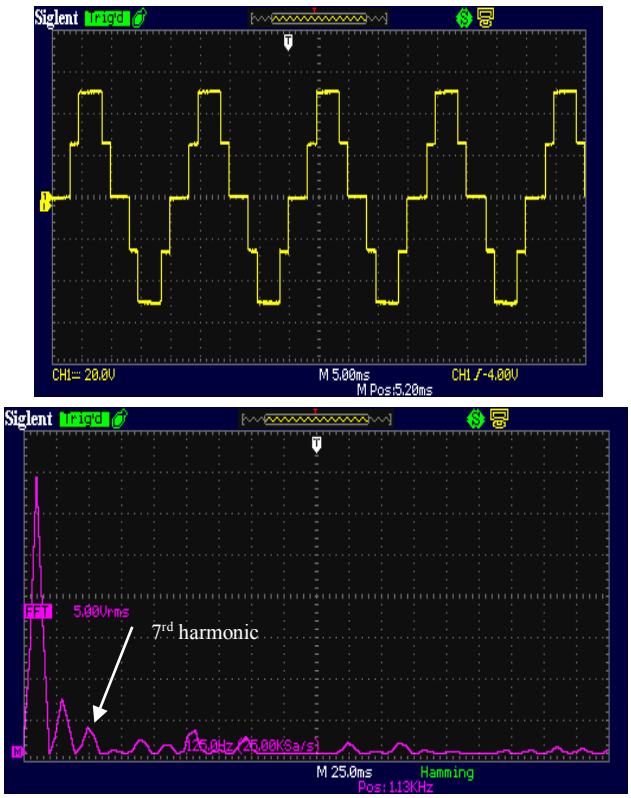


**Fig. 8.** Generated Voltage waveforms (Left) and FFT analysis (Right in the case of eliminating the seventh harmonic for $r = 0.9$.

## 5. CONCLUSIONS

This paper demonstrated the ability of the selective harmonic elimination strategy for multilevel inverters of eliminating any undesired harmonics and maintain the fundamental component at a desired value, and also the possibility of using the simulated annealing algorithm to solve the optimal switching problem for multilevel inverters. The set of non-linear equations that describe the overall system are solved to obtain the optimal switching angles using the proposed optimization algorithm which belongs to the physics inspired optimization methods. The selective harmonic elimination strategy was tested in this paper for multiple situations and different values of modulation index r in order to prove the efficiency of this control method. Simulation and experimental results show a great agreement in this work.

## REFERENCES

[1] Karami, B. Barzegarkhoo, R. Abrishamifar, A. and Samizadeh, M., 2015 .A switched-capacitor multilevel inverter for high AC power systems with reduced ripple loss using SPWM technique, In Power Electronics, Drives Systems & Technologies Conference (pp. 627-632).

[2] Jana, K. C. and Biswas, S. K., 2015. Generalized switching scheme for a space vector pulse-width modulation-based N-level inverter with reduced switching frequency and harmonics, in IET Power Electronics, vol. 8, no. 12, (pp. 2377-2385).

[3] Mistry, T. Bhatta, S. K. Senapati, A. K. and Agarwal, A., 2015, May. Performance improvement of induction motor by Selective Harmonic Elimination (SHE) using Newton Raphson (N-R) method, In International Conference on Energy Systems and Applications (pp.364-369).

[4] Deniz, E. Aydogmus, O. and Aydogmus, Z., 2016. Implementation of ANN-based Selective Harmonic Elimination PWM using Hybrid Genetic Algorithm-based optimization, In Measurement, Vol. 85, (pp. 32-42).

[5] Gnana Sundari, M. Rajaram, M. and Balaraman, S., 2016, April. Application of improved firefly algorithm for programmed PWM in multilevel inverter with adjustable DC sources, In Applied Soft Computing, Vol. 41, (pp.169-179).

[6] Letha, S. S. Thakur, T. Jagdish, K. 2016, July. Harmonic elimination of a photo-voltaic based cascaded H-bridge multilevel inverter using PSO (particle swarm optimization) for induction motor drive, In Energy, Volume 107, (pp. 335-346),

[7] CHABNI, F. TALEB, R. and HELAIMI, M. 2016. Differential Evolution based SHEPWM for Seven-Level Inverter with Non-Equal DC Sources. In International Journal of Advanced Computer Science and Applications (IJACSA), Volume 7 Issue 9 (pp.304-311).

[8] Grobelny, J. and Michalski, R., 2017, March. A novel version of simulated annealing based on linguistic patterns for solving facility layout problems, In Knowledge-Based Systems.

[9] Valdivieso, C. Novillo, F. Gomez, J. and Dik, D., 2016, Centralized channel assignment algorithm for WSN based on simulated annealing in dense urban scenarios, 2016 In 8th IEEE Latin-American Conference on Communications (pp. 1-6).

[10] Raha, S. B. Mandal, K. K. and Chakraborty, N., 2013, Parametric variation based simulated annealing for reactive power dispatch," In IET Chennai Fourth International Conference on Sustainable Energy and Intelligent Systems (pp. 29-34).

[11] Sadiq m. Sait, oughali, f. C. And al-asli, m., 2016,design partitioning and layer assignment for 3d integrated circuits using tabu search and simulated annealing, in journal of applied research and technology, volume 14, issue 1, (pp 67-76).